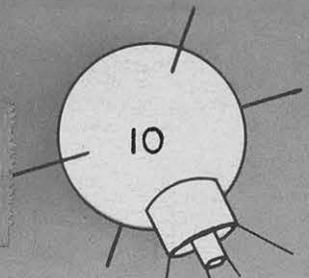

MESOMETEOROLOGY PROJECT

Department of the Geophysical Sciences
The University of Chicago

STUDY OF THE DEVELOPMENT OF PREFRONTAL SQUALL-SYSTEMS USING NSSP NETWORK DATA

by

Joseph L. Goldman

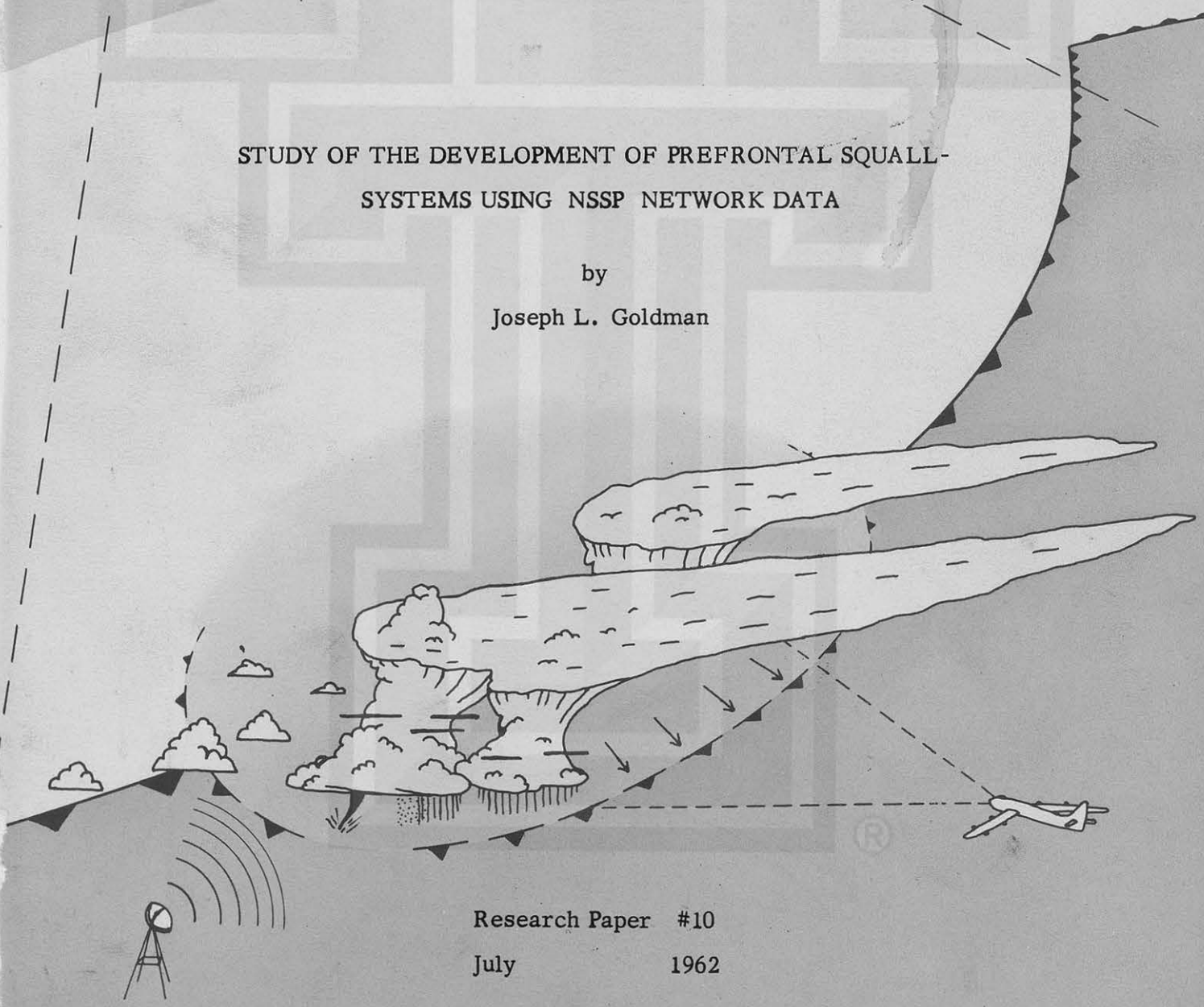

Research Paper #10

July 1962

RESEARCH PAPER #10

MESOMETEOROLOGY PROJECT
Department of the Geophysical Sciences
The University of Chicago

STUDY OF THE DEVELOPMENT OF PREFRONTAL SQUALL-SYSTEMS USING NSSP NETWORK DATA

by

Joseph L. Goldman

This research has been sponsored by the U. S. Weather Bureau under contract Cwb 10201 (NSSP).

TABLE OF CONTENTS

A b s t r a c t

A four dimensional study using all available meteorological data including satellite cloud photographs is made of the atmosphere perturbed by severe storms. In order to study kinematic properties in mesoscale, a method of approximating the hourly upper air wind fields from six hourly data is developed. Precisely rectified TIROS I cloud photographs are also used to estimate kinematic properties of the atmosphere at the cloud level, and a comparison is made of the divergence computed from the cloud-shadow relationships with that computed from the approximated hourly wind field. Composites of the analyses of various meteorological parameters are portrayed for the period of the incipient stage of development of the mesosystem. The use of aircraft measurements of meteorological parameters as an aid to determining necessary boundary conditions at the various stages of the development of severe storms is discussed.

I. INTRODUCTION

In a recent review of analytical mesometeorology Fujita (1962) traced the history of severe storm research from the early days of the development of frontal theory, when data was insufficient to describe most cyclone-scale disturbances, to 1961, when specialized research networks had been in operation to provide data for the study of mesoscale disturbances. In the various analyses shown in this review are seen the distributions of various measured meteorological parameters for particular case studies. Conspicuously absent from the analyses of severe storm cases is an adequate number of analyses of the upper air corresponding to the particular cases. Although this fact is related to the inadequate density of upper air stations for describing mesoscale phenomena, it seems that interest in the variations of the upper air in the mesoscale has not paralleled the interest shown in the description of the various mesoscale phenomena as they appear at the surface.

Due to the discovery, by Whitney and Fritz (1961), that the TIROS I satellite had photographed a square-looking cloud which was related to severe storms, interest developed regarding the utility of extra-terrestrial-based cloud observations for the study of mesoscale phenomena. Since this square-looking cloud mass was found to be within the area covered by the National Severe Storms Project's alpha-network, it was decided that a study would be made of all available meteorological data related to the square-looking cloud. To implement this and future studies using satellite based measurements, Fujita (1961b) developed a method by which satellite cloud photographs could be rectified with sufficient precision to be used in the study of mesoscale phenomena. Since the synthesis and reduction of these data was a formidable task, it was decided that the reduced meteorological data, in plotted form, and the rectified TIROS data be published to avoid any duplication of effort. With the data in the form presented by Goldman and Fujita (1961), it was possible to study compositely meteorological parameters during the various developmental stages of severe storms.

Although more detailed data have become available for more recent cases of severe storms, this study has continued with the purpose of testing various methods of approximation used to obtain mesoscale variations and the utility of heretofore unused types of data.

II. SYNOPTIC SITUATION

From the surface data obtained by the National Severe Storms Project, it is possible to show the synoptic situation in detail. Generally, the large systems are a trough oriented approximately north-south through the Central Plains with a ridge over the Rocky Mountains and the Bermuda High effecting the southeastern United States.

Figures 1 through 5 are the surface mesoscale analyses for the period of investigation of this case. In these figures the cold and quasi-stationary fronts are indicated in the usual manner of the daily weather maps. For purposes of both clarity and brevity the quasi-stationary front in this study will be referred to as the temperature front. The line with spines drawn perpendicular to it represents a moisture front. The side of the line with double spines is the moist side, and the side with the single spine is the dry side, thereby paralleling the definition of the temperature front. A dry front is represented by a line with double spines pointing in the direction toward which the front is moving. Isobars are drawn for 1-mb increments where feasible. The surface wind velocity is indicated in the usual manner with the long barb and pennant equal to 5 and 25 kts respectively. The shorter barbs represent speeds relative to 5 kts in direct proportion to their length. The tornado symbols show the locations of reported tornadoes and the times (CST) of occurrence as determined from the published "Storm Data" and from the remarks in the WBAN 10's of various reporting stations within the area of interest. A tornado symbol with its point removed represents a funnel not touching the ground.

Figure 1 depicts the general quiescent state of the atmosphere prior to the development of the square-looking cloud mass observed by TIROS I at approximately 1400 CST. At 1200 CST, a quasi-stationary front extends southward through central Kansas and western Oklahoma and then northwestward through the Texas Panhandle to the Rocky Mountains. A moisture front extends from near the Red River in western Oklahoma south-southwestward through Texas. By 1500 CST (Fig. 2) a well defined mesosystem had developed in southwest Oklahoma in the proximity of both the temperature and moisture fronts. The line along which the pressure surge occurs is

shown in this and other figures as a dashed line. Spikes pointing in the direction of motion indicate appreciable values of the local pressure change. The stippling indicates areas of hourly accumulated precipitation greater than one half inch. The heavy stippling represents an hourly accumulation of one inch or greater. The space gradient between these implied isohyets was determined using the plot of instantaneous rate of precipitation (Goldman and Fujita, 1961).

As can be seen in Fig. 2, at 1600 CST and later, tornadoes were reported in Oklahoma and Kansas. Since the tornadoes in Kansas occurred on the edge of the NSSP network, any organized effect of the tornadoes was not discernible in the recorded data. An interesting feature of the pressure pattern of 1500 CST is the small area of low pressure near the southern intersection of the front and the meso-system boundary. This low pressure region remained about the intersection point throughout the period of investigation.

By 1800 CST the mesosystem associated with the square-looking cloud mass had expanded and moved so that it influenced most of western Oklahoma (Fig. 3). A second mesosystem had developed in the low pressure region south of the first system and east of the moisture front. A cold front located north of the temperature front began moving rapidly southward and eastward. Figures 4 and 5 show the progression of these systems and fronts throughout the remainder of the period of analysis.

By 2100 CST there were some indications of a system developing within the first system. However, the proximity of the boundary of this newer system to the edge of the network precluded the detailed analysis necessary to define a new system. A dry front, along which significant drops in dew-point temperature were observed, had developed in western Texas and by 2400 CST had overtaken the moisture front. The pressure pattern within the first system retained its large gradient due to the continuous development of intense precipitation near the boundary. The relatively flat pressure gradient was probably due to the large area of precipitation of lesser intensity west of the boundary. The precipitation pattern of the second system reamined restricted to a narrow band of high intensity throughout the period of analysis. This fact would explain the retention of its characteristic pressure pattern even while totally within the first system (Fig. 5).

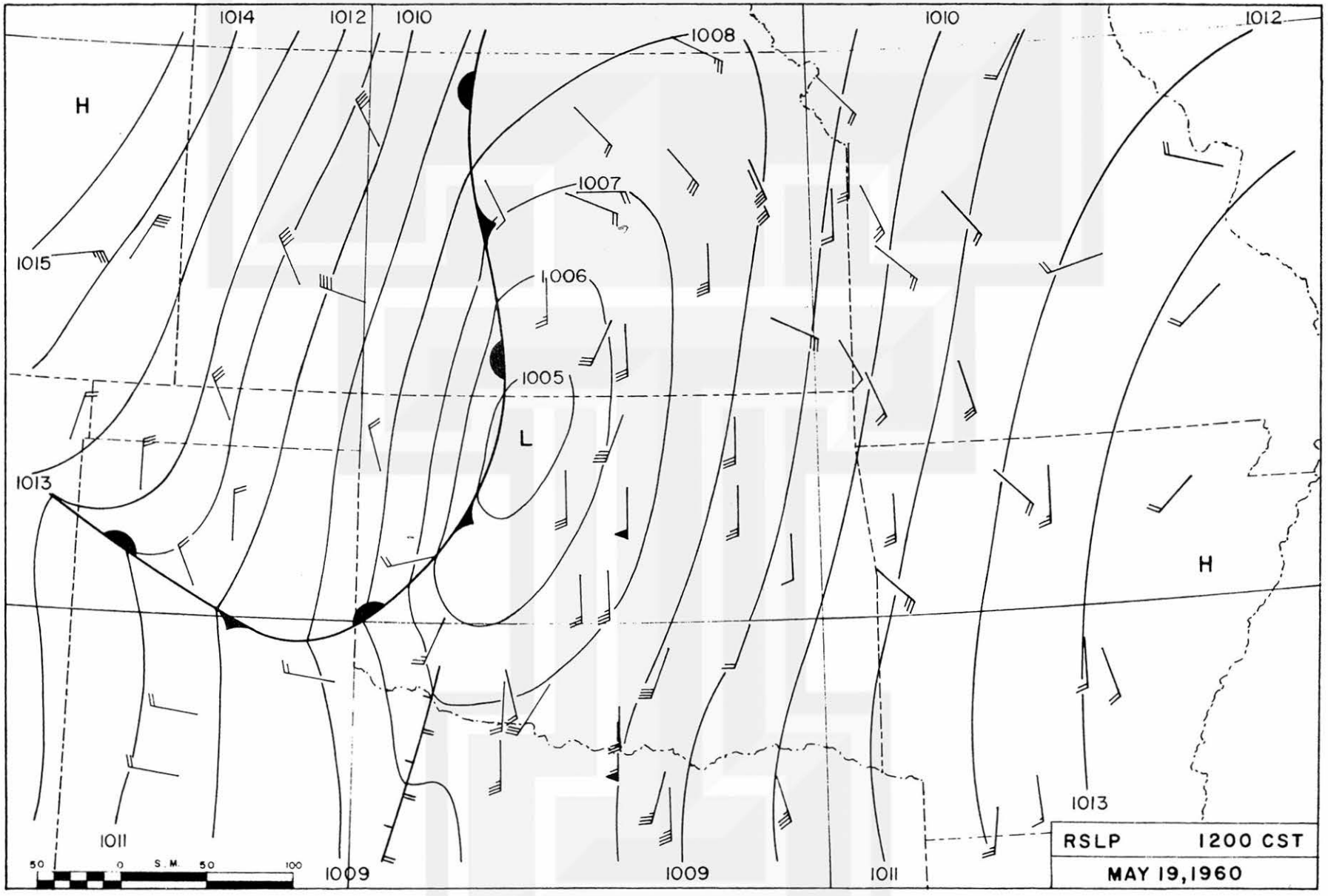

Fig. 1 Reduced sea level pressure analysis, reported surface winds and surface positions of fronts at 1200 CST.

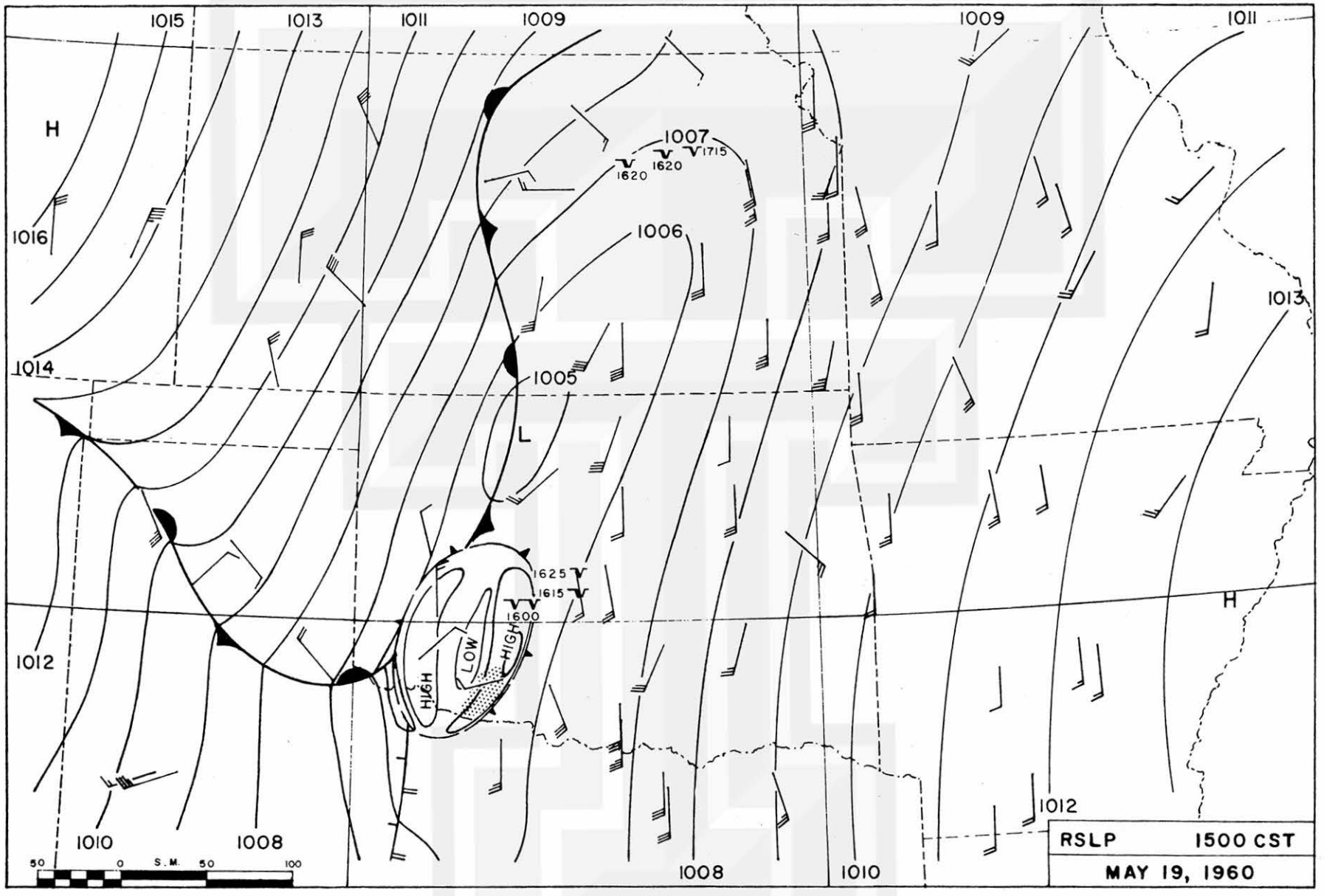

Fig. 2 Reduced sea level pressure analysis, reported surface winds, surface positions of fronts, hourly precipitation analysis (stippled area is region where precipitation accumulation is greater than 1/2 inch per hour), tornadoes within 3 hr of 1500 CST.

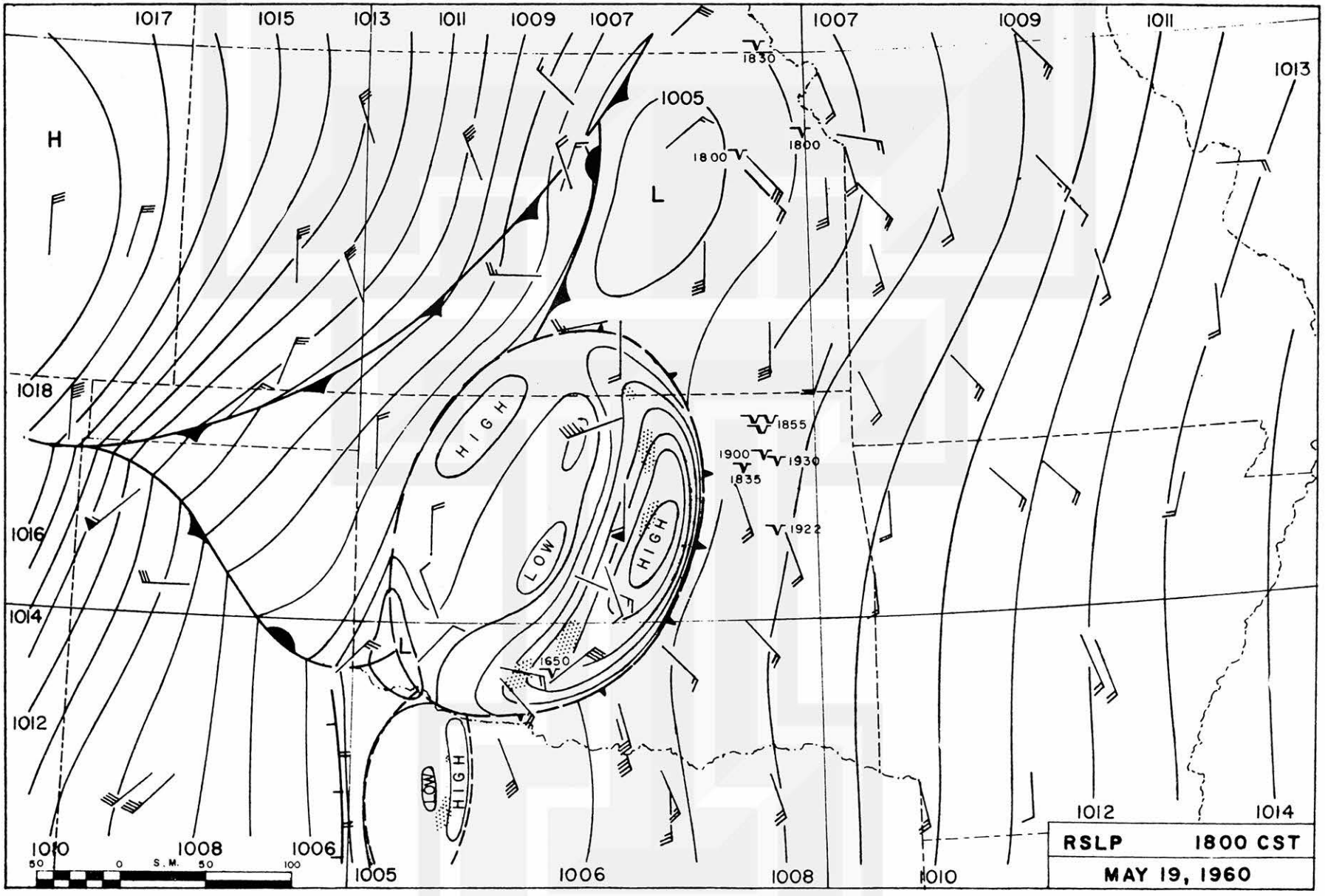

Fig. 3 Reduced sea level pressure analysis, reported surface winds, surface positions of fronts, hourly precipitation analysis (stippled area is region where precipitation accumulation is greater than 1/2 inch per hour, heavy stippling denotes greater than 1 inch per hour), tornadoes within 3 hr of 1800 CST.

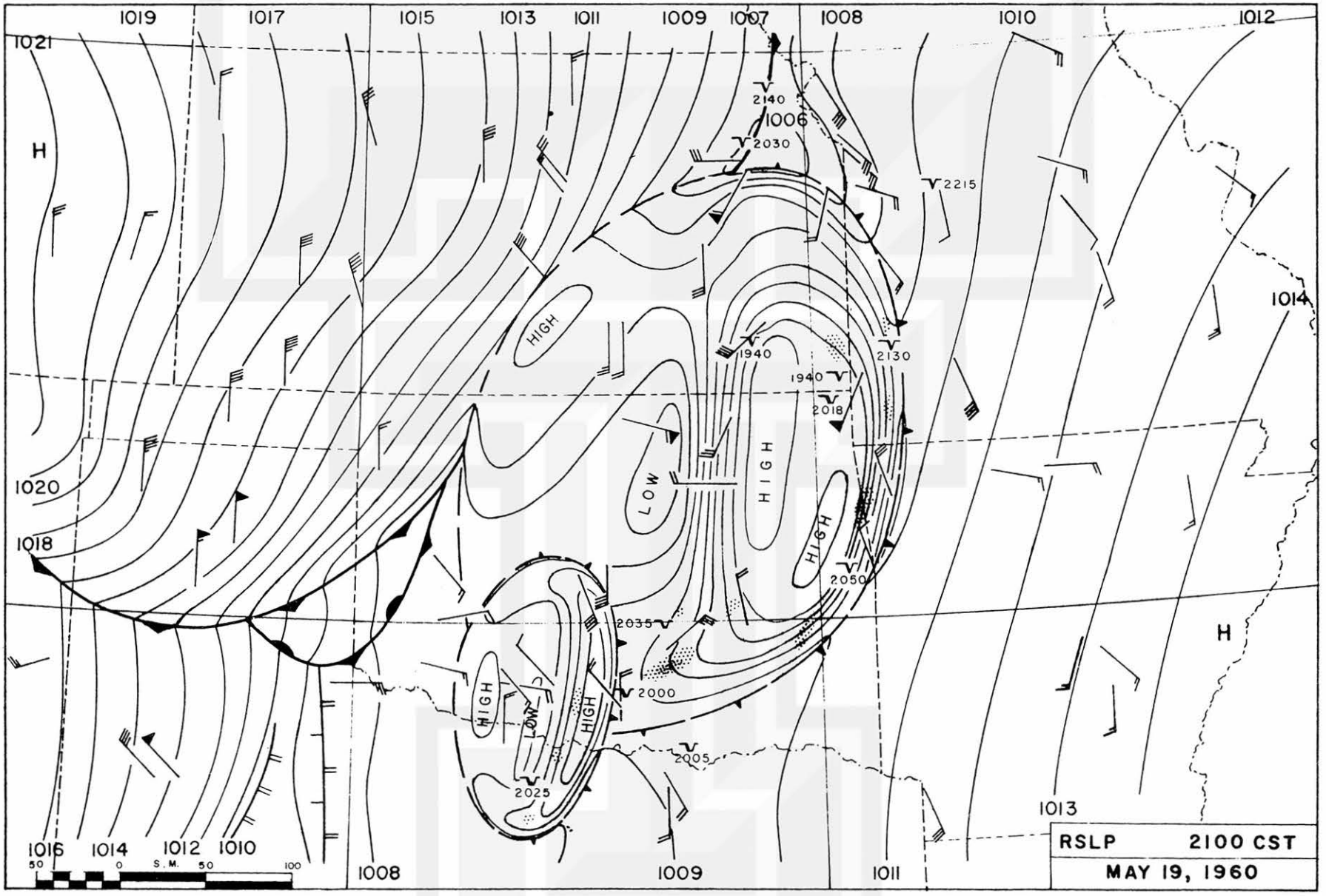

Fig. 4 Reduced sea level pressure analysis, reported surface winds, surface positions of fronts, hourly precipitation analysis (stippled area is region where precipitation accumulation is greater than 1/2 inch per hour, heavy stippling denotes greater than 1 inch per hour), tornadoes within 3 hr of 2100 CST.

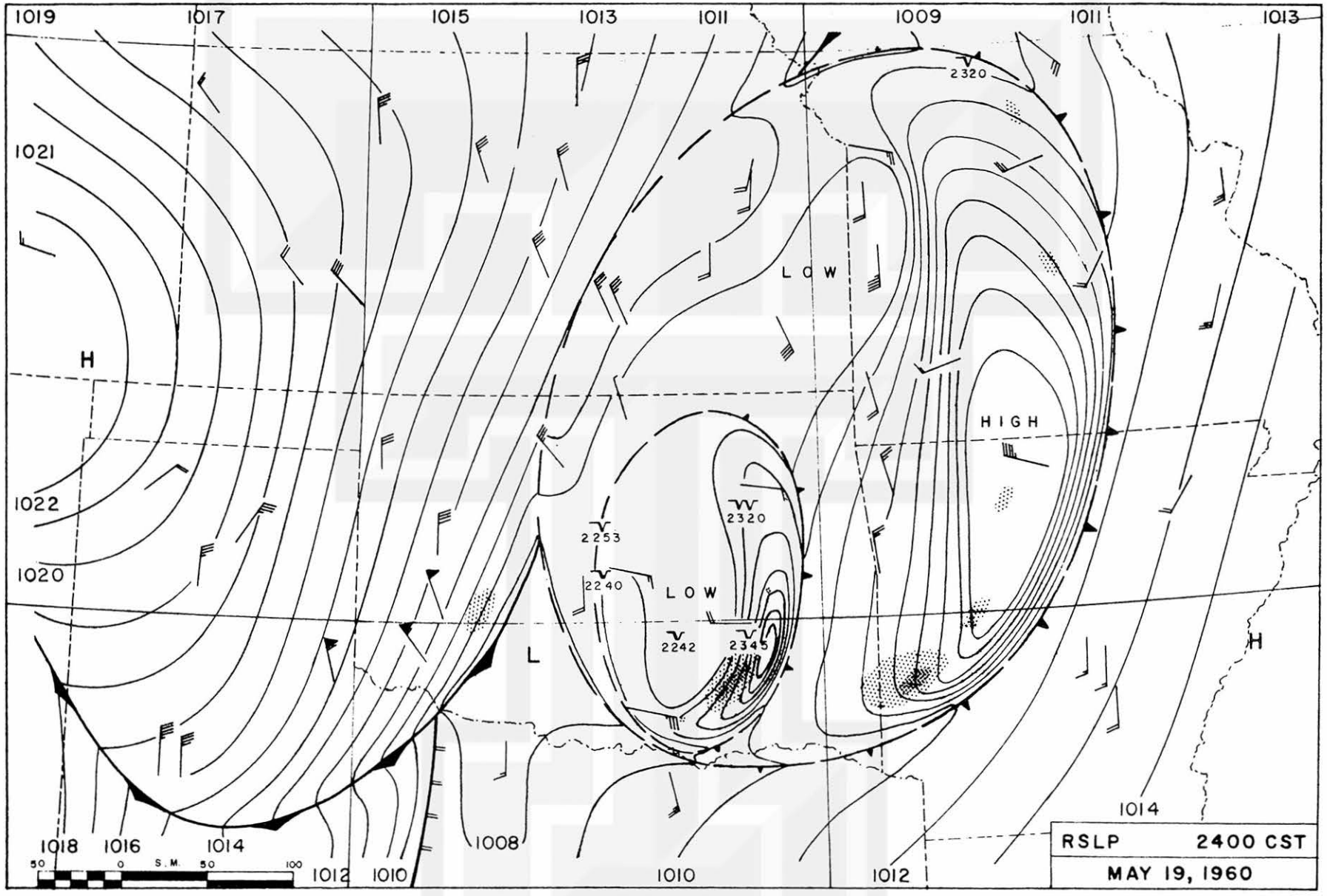

Fig. 5 Reduced sea level pressure analysis, reported surface winds, surface positions of fronts, hourly precipitation analysis (stippled area is region where precipitation accumulation is greater than 1/2 inch per hour, heavy stippling denotes greater than 1 inch per hour), tornadoes within 3 hr of 2400 CST.

III. UPPER AIR

In order to test the utility of the upper air data in describing mesoscale variations, streamlines and isotachs were drawn for the eight mandatory constant pressure surfaces from 850 mb through 150 mb for each of the synoptic hours, 0600, 1200, 1800, and 2400 CST. During the 12-hr period of surface analysis the mesosystems influenced a region within which there was more than one radiosonde station. It was therefore believed that an analysis of the time variations of the total wind vectors at specific points would show mesoscale features that would not be seen readily in analyses separated by 6-hr intervals. On the resulting 32 charts the wind speed and direction were read at grid points formed by the intersections of longitudes and latitudes two degrees apart. Wind vectors at each grid point for the four synoptic data times were then plotted on eight composite charts.

In order to check the consistency of composite winds at each constant pressure surface, it was decided that hodographs be drawn at each grid point. To avoid any abrupt changes in the wind velocity, smooth curves, instead of straight lines, were used to connect the heads of the vectors (Fig. 6). These curves could also be checked for consistency, since in the large scale pattern the curves of adjacent data points would not be expected to show large differences in shape, except near troughs, wedges, and inflection points in the streamline pattern.

The analyses of streamlines and isotachs for the eight mandatory constant pressure surfaces at 1800 CST are shown in Figs. 7 through 14. If reference is made to the plotted constant pressure data (Goldman and Fujita, 1961), the only major difference between the analyses and the plotted data is in the region of the Oklahoma City rawinsonde station (OKC). A perusal of the recorder record for OKC at 1800 CST shows that the balloon was most likely influenced by the vertical motions within the reported overcast of cumulonimbus mammatus. However, the recorded elevation angles of the rawin show decreases to below 10 degrees of elevation above the 850-mb surface. In fact the elevation angles continually decreased to the lowest value

(7.82 degrees), which was attained at 644 mb. In addition, due to the erratic spacing between contacts, the computed winds from the sounding are questionable. When the wind field is viewed on the composite time plots, the perturbation of streamlines and isotachs at 1800 CST near OKC was not evident in any other region at later hours. The 1800 CST reports of OKC were therefore not used in the analyses shown.

A contour analysis of the eight constant pressure surfaces shows a small trough in the region of OKC above 850 mb. At 850 mb a slight wedge in the contours is observed.

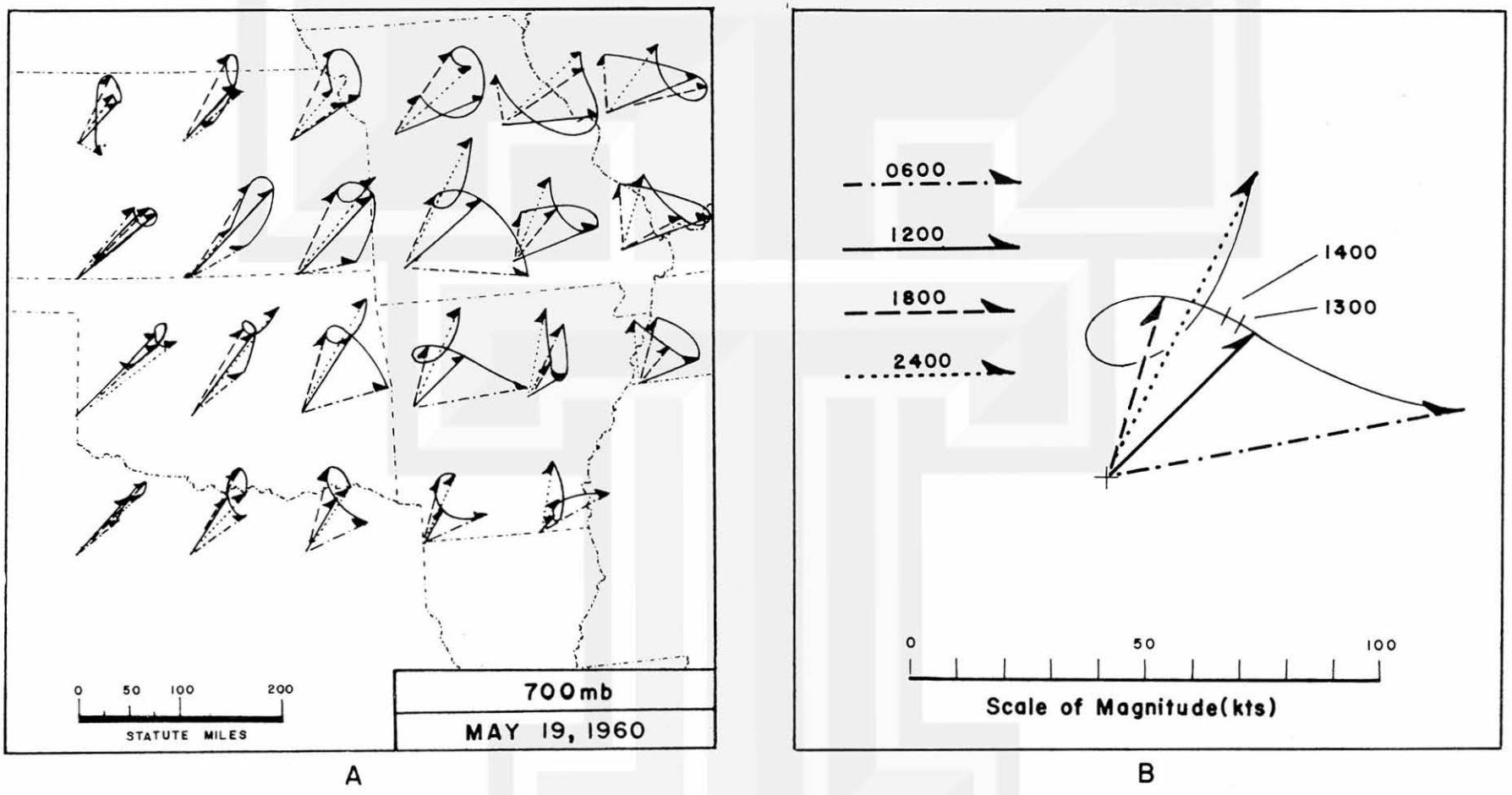

Fig. 6 Composite time plot of wind vectors at grid points. A - Wind vectors with smooth curve connecting the heads of the vectors. B - Model showing the approximation to the hourly wind between vectors.

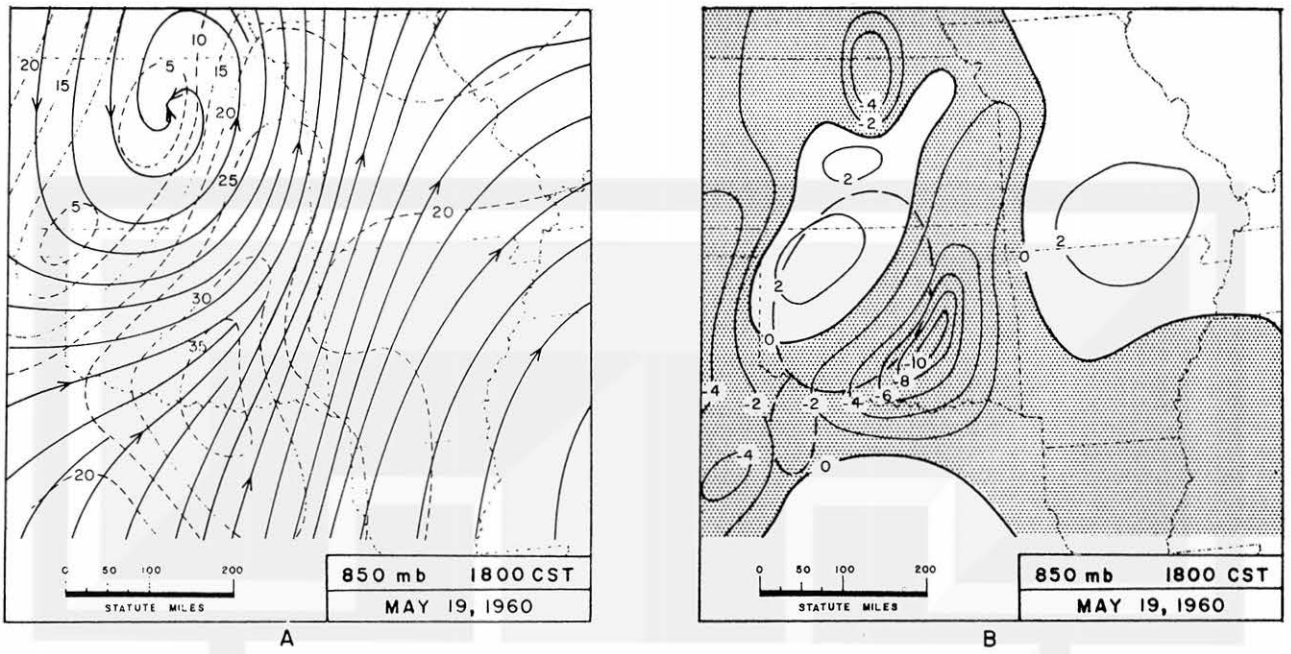

Fig. 7 Upper air kinematics. A - Streamlines (solid) and isotachs (dashed lines) at 5-kt intervals. B - Isolines of divergence ($x10^{-5}$ sec^{-1}) with surface boundary of mesosystems (dashed lines), stippled area is region of convergence.

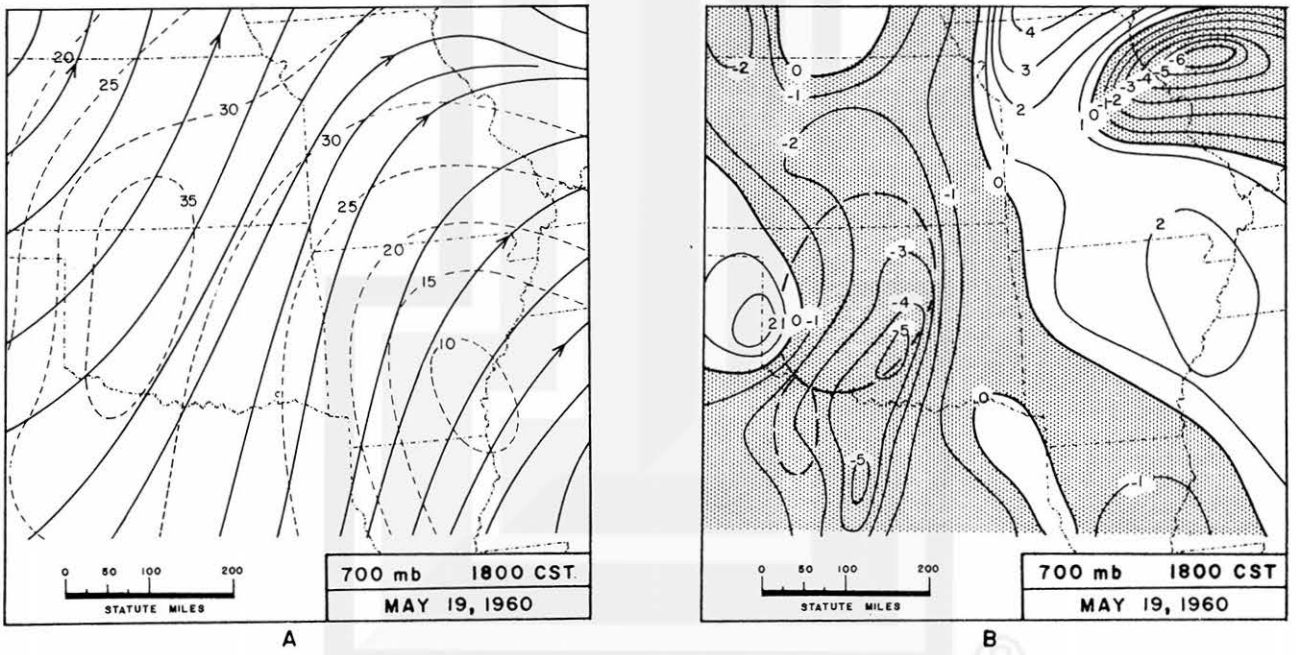

Fig. 8 Upper air kinematics. A - Streamlines (solid) and isotachs (dashed lines) at 5-kt intervals. B - Isolines of divergence ($x10^{-5}$ sec^{-1}) with surface boundary of mesosystems (dashed lines), stippled area is region of convergence.

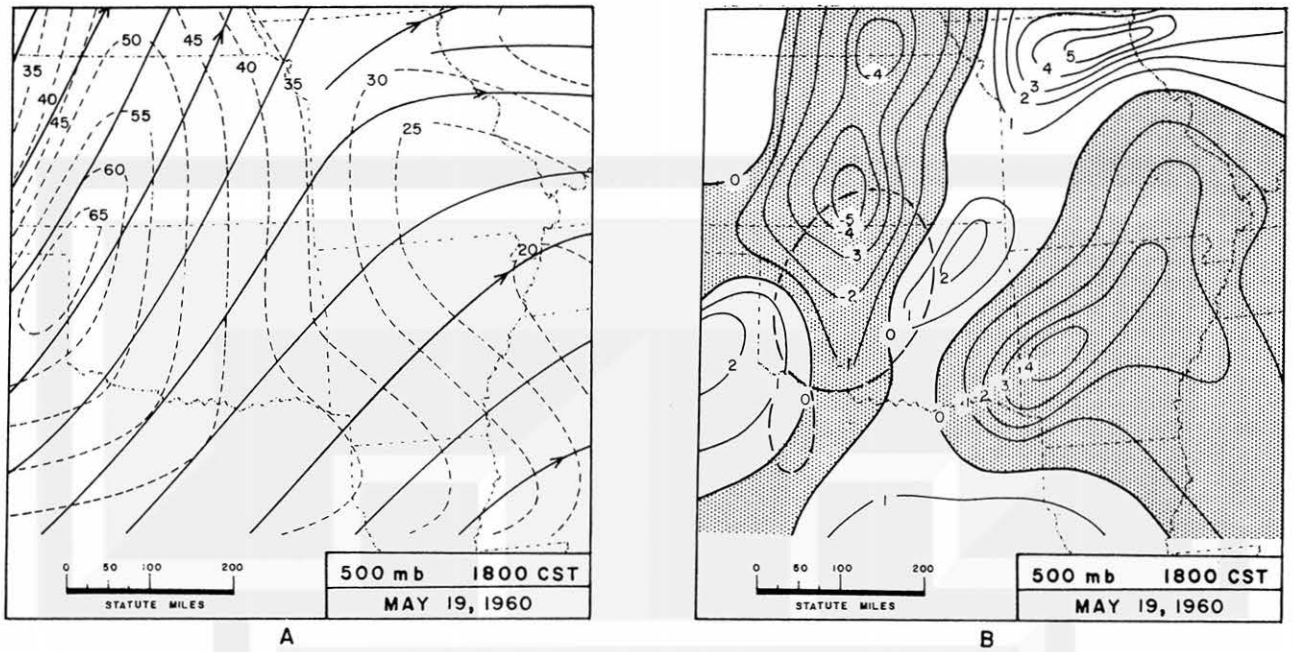

Fig. 9 Upper air kinematics. A - Streamlines (solid) and isotachs (dashed lines) at 5-kt intervals. B - Isolines of divergence (x10^{-5} sec^{-1}) with surface boundary of mesosystems (dashed lines), stippled area is region of convergence.

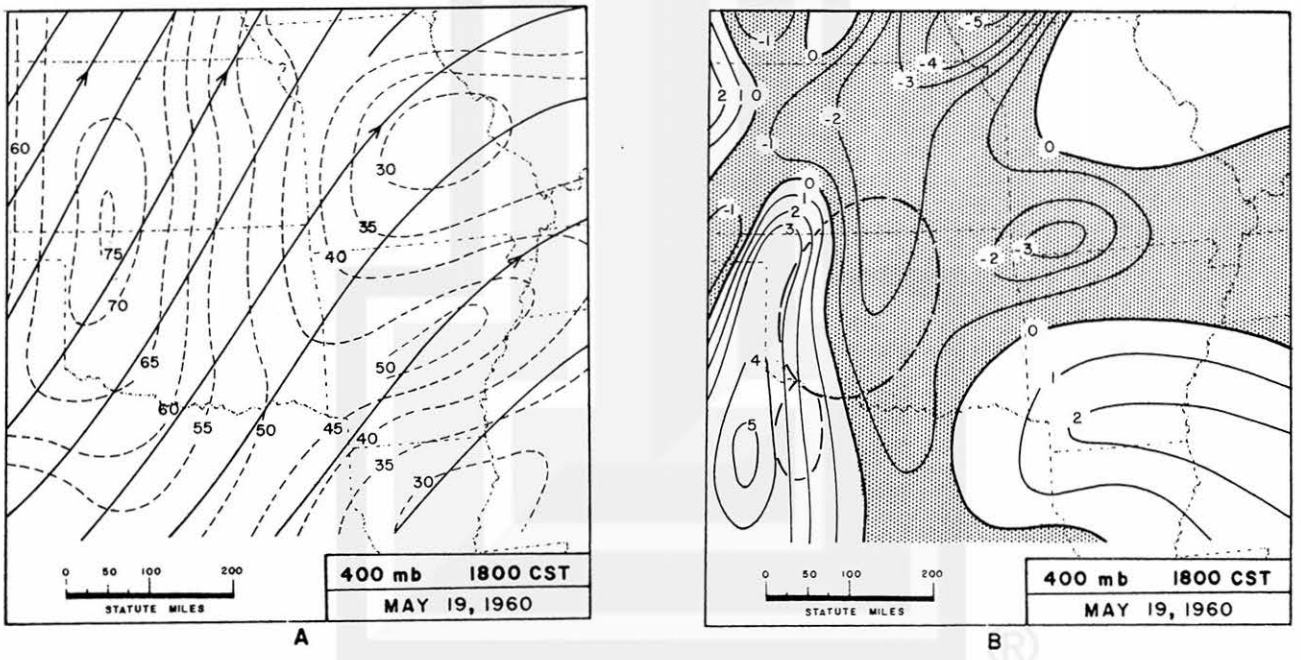

Fig. 10 Upper air kinematics. A - Streamlines (solid) and isotachs (dashed lines) at 5-kt intervals. B - Isolines of divergence (x10^{-5} sec^{-1}) with surface boundary of mesosystems (dashed lines), stippled area is region of convergence.

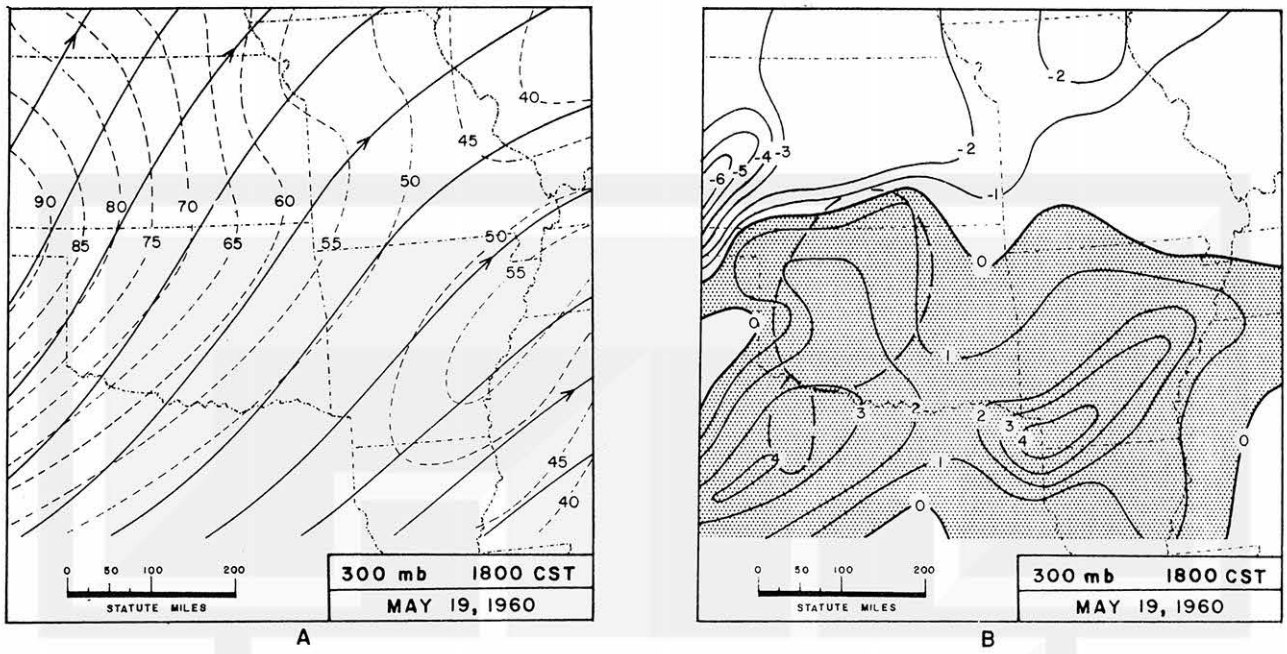

Fig. 11 Upper air kinematics. A - Streamlines (solid) and isotachs (dashed lines) at 5-kt intervals. B - Isolines of divergence ($x10^{-5}$ sec^{-1}) with surface boundary of mesosystems (dashed lines), stippled area is region of divergence.

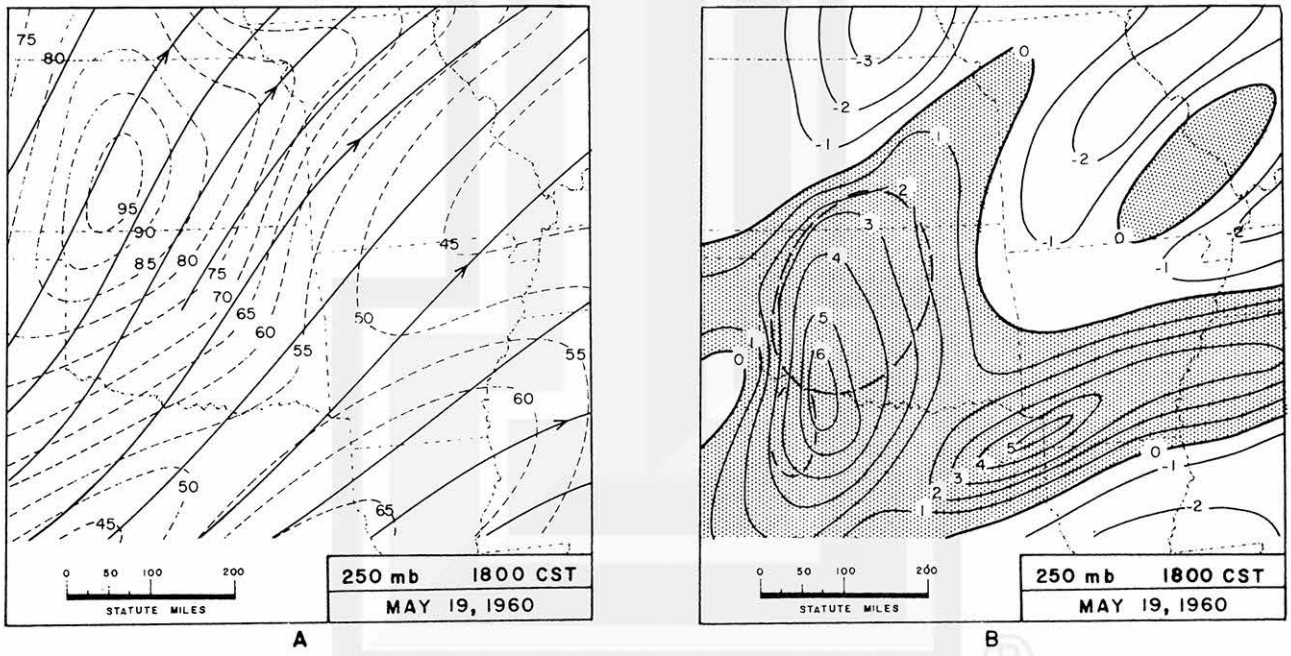

Fig. 12 Upper air kinematics. A - Streamlines (solid) and isotachs (dashed lines) at 5-kt intervals. B - Isolines of divergence ($x10^{-5}$ sec^{-1}) with surface boundary of mesosystems (dashed lines), stippled area is region of divergence.

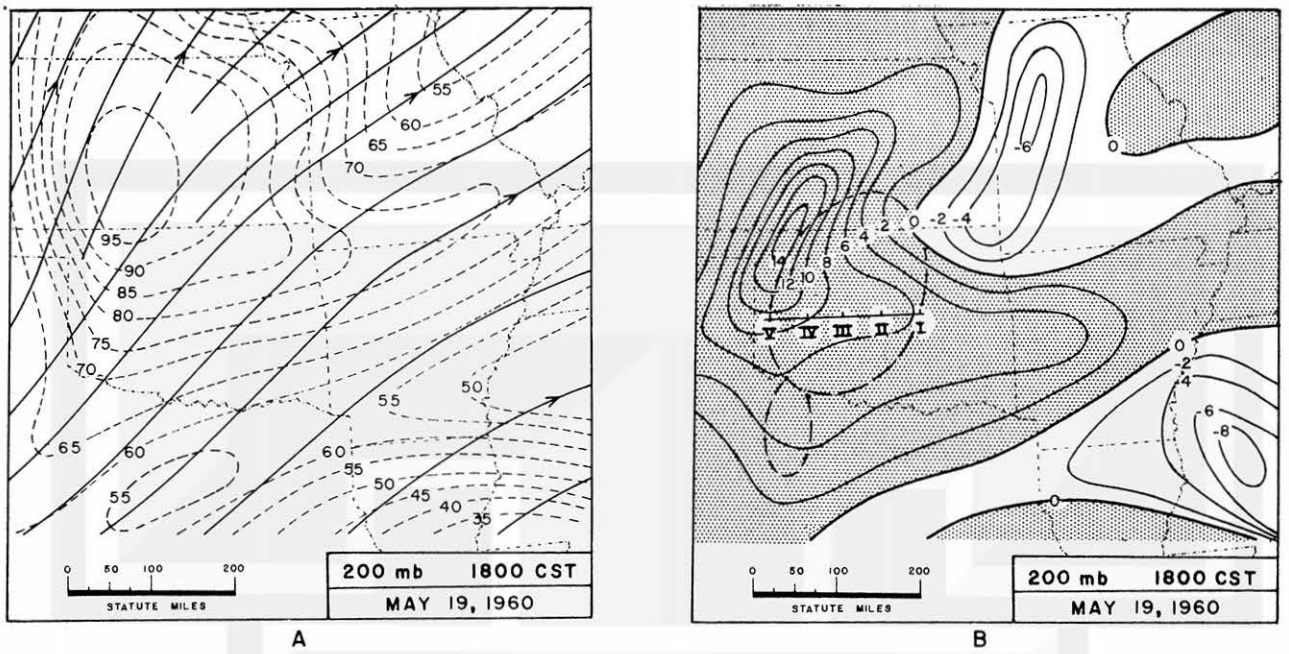

Fig. 13 Upper air kinematics. A - Streamlines (solid) and isotachs (dashed lines) at 5-kt intervals. B - Isolines of divergence ($x10^{-5}$ sec^{-1}) with surface boundary of mesosystems (dashed lines), stippled area is region of divergence. Numerals on cross-section line show locations of profiles.

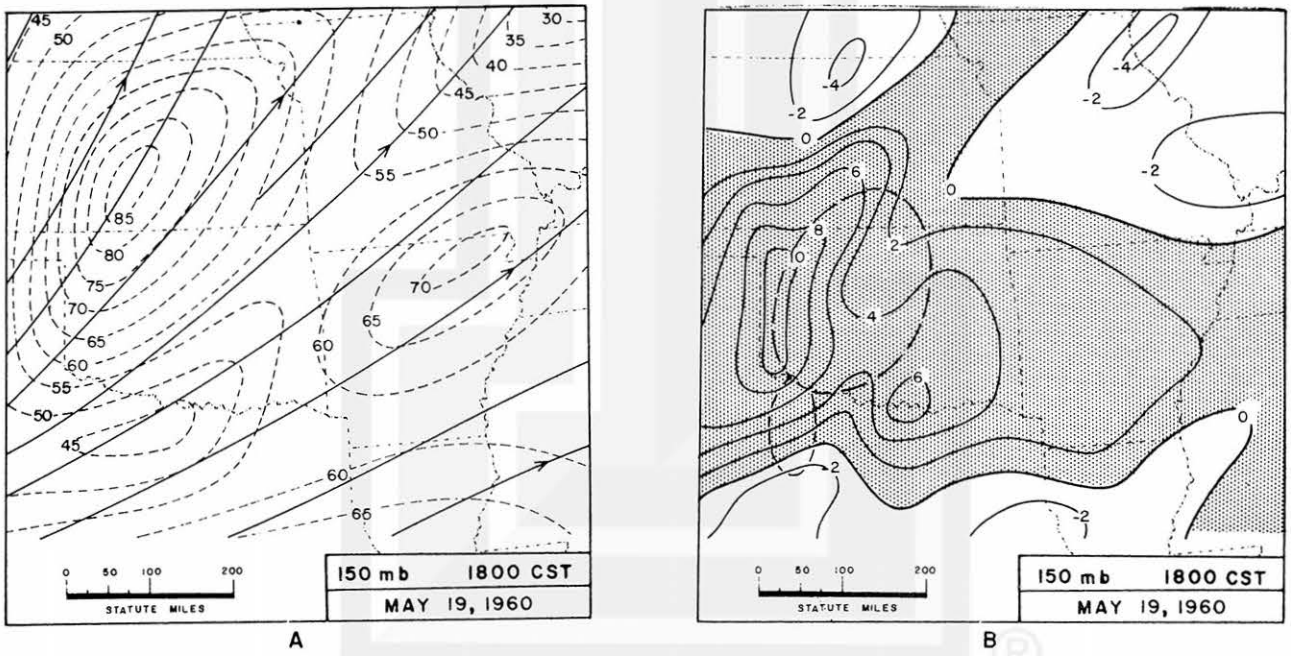

Fig. 14 Upper air kinematics. A - Streamlines (solid) and isotachs (dashed lines) at 5-kt intervals. B - Isolines of divergence ($x10^{-5}$ sec^{-1}) with surface boundary of mesosystems (dashed lines), stippled area is region of divergence.

IV. COMPUTATION OF DIVERGENCE

In order to study the kinematics of mesoscale motion, a method of computing divergence was sought that would extract the maximum amount of information from the observed data. Since the data had been checked for consistency by the methods discussed above, and, in the process of these checks, reliable streamline and isotach fields had been drawn, it was decided that the general kinematic method be used to compute the divergence field from which the vertical motion field could then be derived.

Tests of various methods of divergence computation have been made (Panofsky et al.) and the present thoughts on the matter of the quantitative results of divergence computations are conflicting. Therefore three tests, using differing techniques, were performed on the computation of divergence. The case used to test the various techniques was the wind field at the 150-mb surface for 0600 CST, May 19, 1960. The test consisted of comparing the amount of detailed information derived from the wind field by the computation of divergence using a constant grid size with that using a variable grid size developed by Fujita (1955). The constant grid method involved reading the wind direction with respect to the grid and speed at grid points 150 km apart. It also involved computing the components of the wind along the orthogonals of the grid and performing the operation:

$$\frac{\delta u}{\delta x} + \frac{\delta v}{\delta y} = \mathrm{div}\ V$$

where u and v are the components of the total wind, V, along the x and y axes, respectively. Since the map used was the standard Lambert Conformal, and since the area of computation was between 30 and 40 degrees north latitude, the distortion factor was considered negligible; it was, therefore, not taken into account.

Since the utilization of a digital computer for the computation of divergence was considered, the speed with which the computation could be made was also studied. The program devised for the computer consisted of a wind direction and speed for each grid point as input data, and the output would be divergence and vorticity. Since the breakdown of the wind velocity into its components was done in the program, the time involved would be almost entirely consumed in the reading and coding of input data.

Two tests were made using the grid method devised for a machine computation. The input data for the first test consisted of wind directions to the nearest five degrees, which could be read off the streamline pattern directly. For the second test, wind directions to the nearest degree were read off an isogon analysis. The wind speeds were measured in both tests from the isotach pattern to the nearest knot. The ensuing analyses were then compared to an analysis based on the method developed by Fujita.

The analyses and resulting computations are shown in Figs. 15, 16, and 17. Figure 15 is the 150-mb analysis of streamlines and isotachs with the analysis of divergence computed from the Fujita method. Figure 16 is the analysis and plot of divergence as computed from wind directions to the nearest five degrees. Figure 17 is the same as 16, but from wind directions to the nearest degree. The ratio of the time required to produce the values in Fig. 16 to that in Fig. 17 is approximately two-thirds. When this time factor is weighted by the reduction in human error (brought about by reading from a field rather than reading from a tangent drawn at a point), the accuracy achieved seems worth the extra time. The time required to draw orthogonals to the streamlines and make the computation using the mechanical device developed by Fujita was nearly equivalent to the time required to draw isogons and read and code the data at grid points. The difference in the amount of time taken for the computation of Figs. 17 and 15 is therefore negligible.

As can be seen in the analysis in Fig. 15, a larger amount of detail can be obtained using the Fujita method since the areas used in the computation can vary discriminately according to the areas of interest. A reduction in grid size to obtain this detail would consist of either a separate computation or a proportionate increase in the total number of grid points which would, in turn, proportionately increase the total time

factor of the computation. The method developed by Fujita was therefore used in the computation of divergence in this study. The analyses of divergence (units, 10^{-5} sec^{-1}) for 1800 CST are shown in Figs. 7 through 14.

Since the purpose of the divergence computation, in addition to obtaining the time variability of the divergence, was to achieve a meaningful representation of the vertical motion related to a mesoscale disturbance, profiles of the vertical motion were obtained at points on the cross-section line shown in Fig. 13. It can be shown that

$$\frac{\partial u}{\partial x} + \frac{\partial v}{\partial y} = -\frac{\partial \omega}{\partial p},$$

where u, v, and p have their usual meteorological meaning, and $\omega \equiv \frac{dp}{dt}$ is the component of motion normal to the pressure surface (Petterssen, 1956).

Using this relation, the slopes of the curve of ω were drawn at the eight pressure surfaces on a p vs. ω chart. In Fig. 18 are the profiles of ω at the specified points along the cross-section line of Fig. 13. The profile was obtained by drawing a smooth curve of the eight values of $\frac{\partial \omega}{\partial p}$ and then drawing the ω profile from the slopes. The absolute values of ω would be determined by an assumed value at the ground or possibly at the tropopause.

There remain questions concerning the slope of the tropopause in the vicinity of both organized squall lines and individual thunderstorm clouds. Therefore, although ω can be considered zero near the tropopause for some large scale problems, ω in a mesoscale system at the tropopause must remain indeterminant. This leaves the ground surface as the boundary value of the vertical motion.

The first approximation to the value of ω at the ground surface could be determined from the slope of the terrain with respect to the isobaric surface. However, in cases where the slope of the terrain is appreciable, sea level isobars would intersect the ground surface. In such cases, use of the continuity equation in the x, y, z - space would be preferable, with suitable adjustments made for the contribution of the terrain's slope to the boundary value of $w = 0$ at a level surface.

Another rather important effect on the computation of divergence in the lower

levels, say between the surface and 850 mb, is the effect of frictional retardation of the wind. Since, in general, frictional retardation is directly related to the wind speed, then divergence computed by the method used in this study would be effected by the increasing frictional effect on the same value of downstream wind shear. For example, the shear related to a value of divergence for a given area when acted upon by frictional retardation would not produce the same gradient of divergence with an increase in downstream shear. The effect on the gradient of the divergence would be a decrease related to the frictional retardation. The preceding example assumes no change in the proportionality factor, which generally does change with differing characteristics of the surface and under varying turbulent conditions of the atmosphere due to surface heating. Although these variations had been considered microscale in character, not effecting the general calculations made of cyclone scale disturbances, their importance increases as interest approaches the small scale variations that are depicted in the study of the various stages of mesosystems.

A possible method of determining these effects in future studies would be to plot the change of the wind profile due to frictional and heating effects at various data points in the area. From the distribution of these values a correlation to the topography and uneven surface heating would be made. Using this correlation a suitable transition from the frictionally effected divergence to the relatively frictionless divergence aloft could be made by considering the scale of physical changes taking place in the atmosphere. This scale would be dependent on the time and space density of data points.

Since data of the sort described above were not available for this study, the profiles of ω represent the relative changes that could be expected from a detailed analysis of existing data. Since other than existent methods of obtaining such data and possibly more elaborate instrumentation are necessary, the solution to the problem of proper boundary values and transitions in the lower levels must await future research.

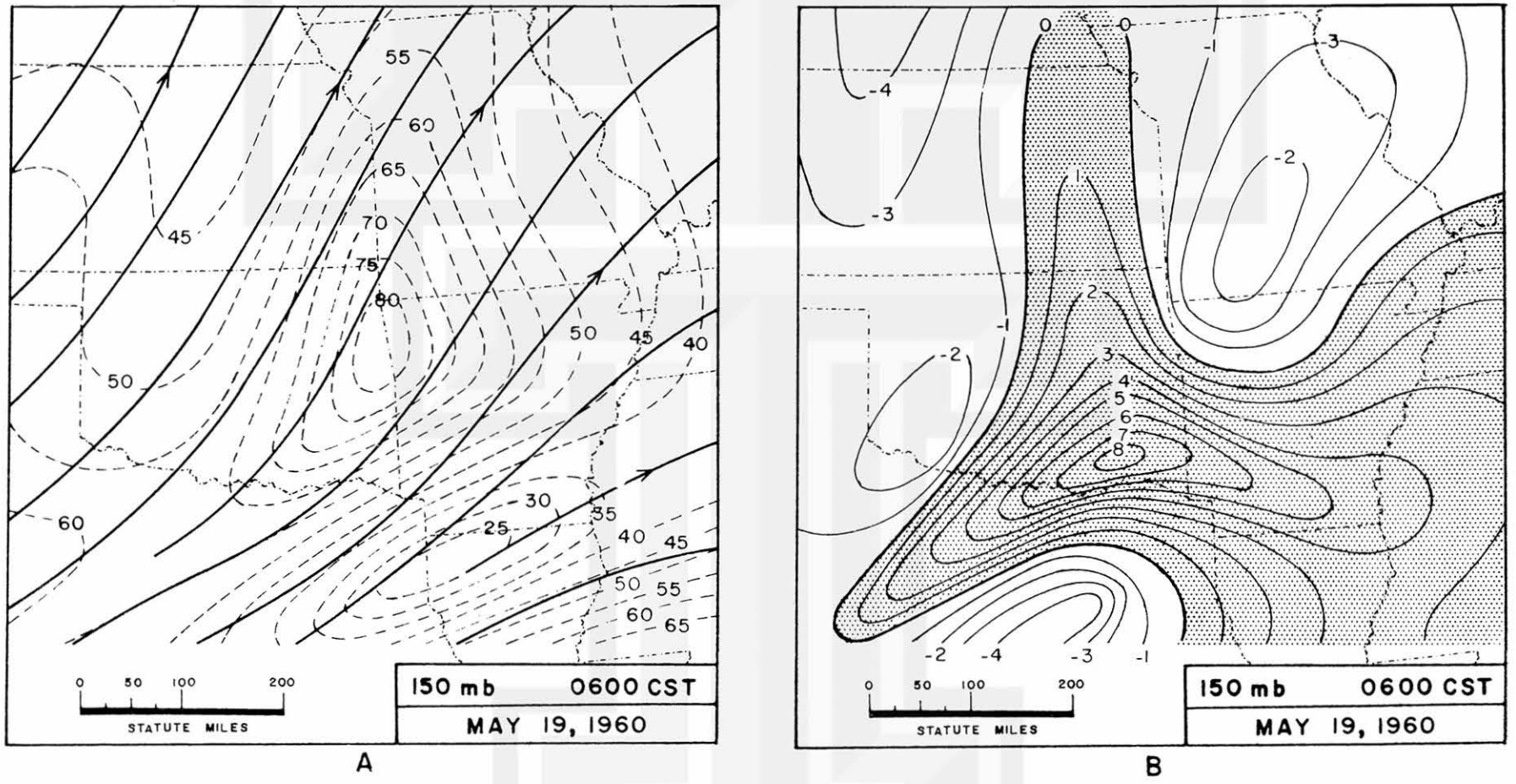

Fig. 15 Test of divergence computation. A - Streamlines (solid) and isotachs (dashed lines) at 5-kt intervals. B - Isolines of divergence ($x10^{-5}$ sec^{-1}) determined from the computations using Fujita's method. Region of positive divergence is stippled.

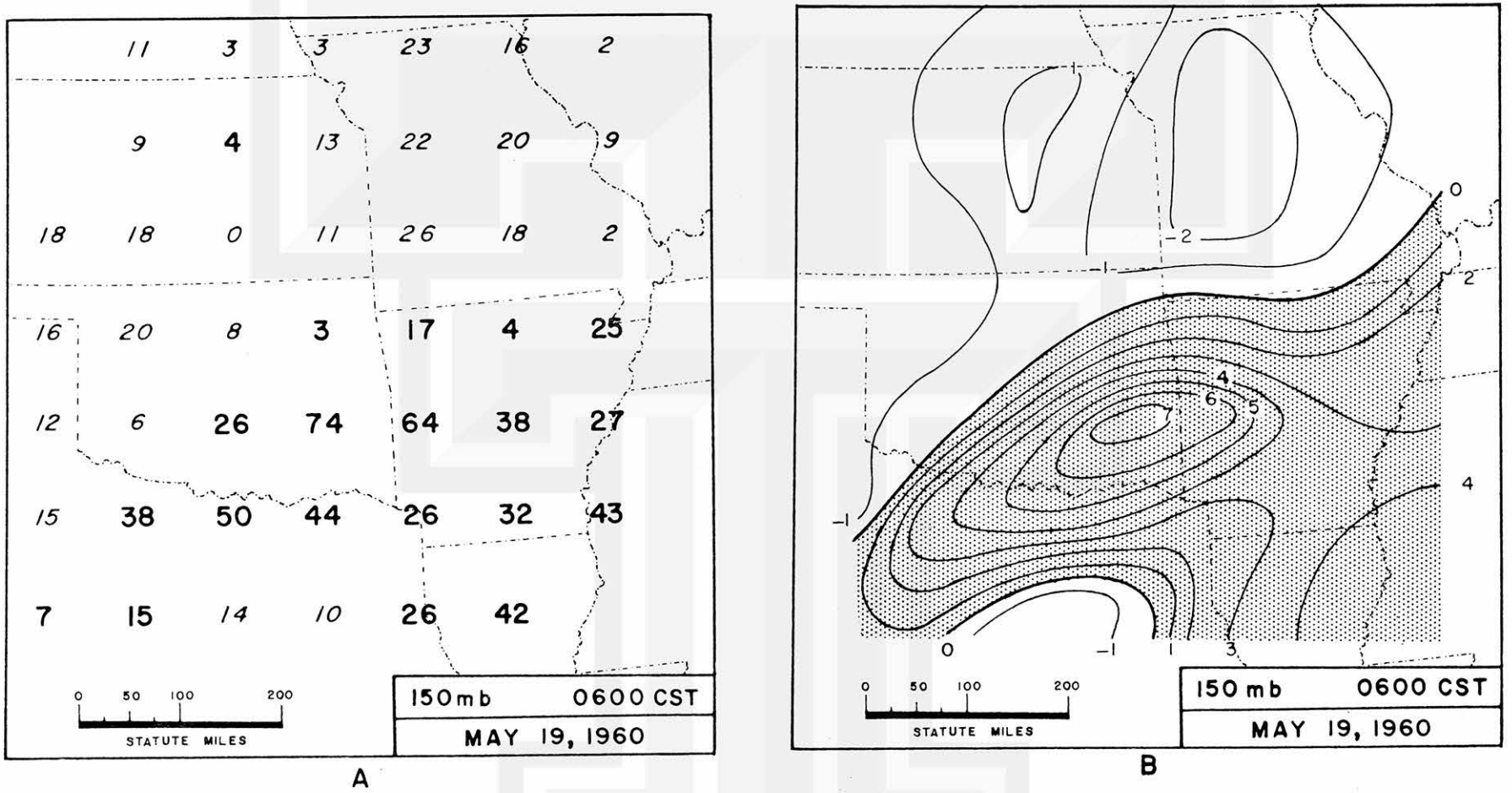

Fig. 16 Test of divergence computation. A - Values of divergence computed at grid points from wind directions to the nearest 5 degrees (bold numbers are positive). B - Isolines of divergence ($x10^{-5}$ sec^{-1}) drawn for the values in A. Region of positive divergence is stippled.

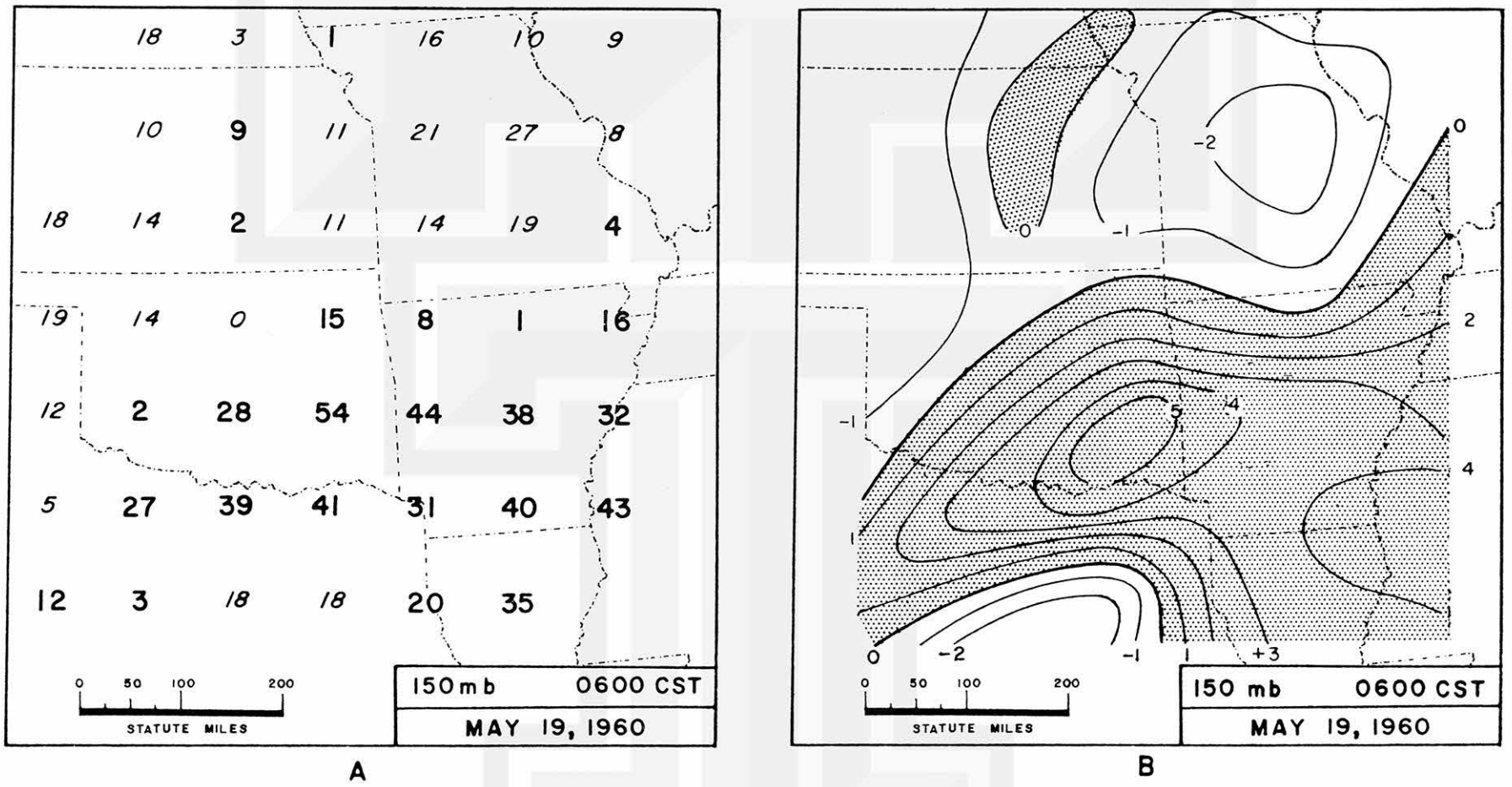

Fig. 17 Test of divergence computation. A - Values of divergence computed at grid points from wind directions to the nearest degree (bold numbers are positive). B - Isolines of divergence ($x10^{-5}$ sec^{-1}) drawn for the values in A. Region of positive divergence is stippled.

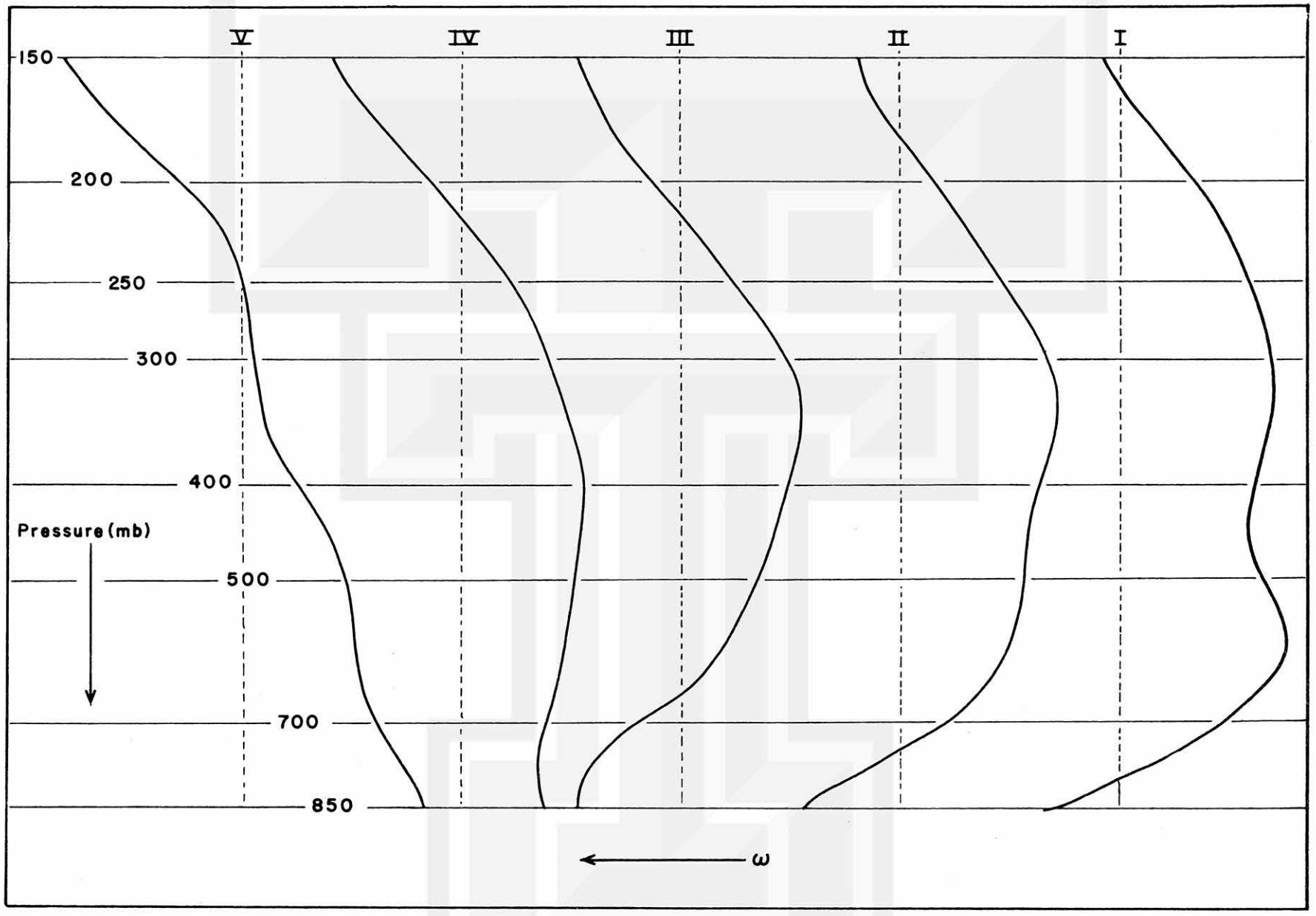

Fig. 18 Profiles of ω for 1800 CST at indicated points on the cross-section line of Fig. 13. Positive slope denotes an increase in upward motion or a decrease in downward motion with height. Vertical dashed lines denote the location of the profiles along the cross-section line and are not to be considered a specific value of ω.

V. THE INCIPIENT STAGE OF THE MESOSYSTEM

A study of the initial developments in the first mesosystem was greatly enhanced by the precise rectification of the TIROS cloud photographs. With the knowledge that a seemingly dense cloud existed over a region where a number of NSSP network stations were measuring temperature, it was postulated that the cooling effect of the cloud shadow should be reflected in the temperature traces of these stations. This hypothesis was confirmed by abrupt decreases in recorded temperatures of the order of one or two degrees Fahrenheit. The times of occurrence of this temperature change and isochrones of temperature drop were then drawn.

In Fig. 19 are the isochrones of temperature drop (solid lines) for the stations within the area of interest. The large circles show the locations of the Weather Bureau and cooperative stations that take visual observations. The types of clouds and amounts of sky covered with the reported surface wind are indicated at these stations. The locations of the network stations are indicated by the small circles. The temperature traces were converted to a space change in the manner shown in the figure. The stippled areas are the regions covered by clouds as indicated by rectified TIROS photographs. The solid areas are the photographed radar echoes shown on the Wichita Falls Radar (SPS) at 1358 CST.

From the declination of the sun on May 19, 1960, the displacement of the cloud shadow from the vertical was found to be approximately two miles. This is true if the cloud mass producing the shadow is assumed to be at an altitude between 30,000 and 40,000 ft. An altitude of 38,000 ft was questionably indicated in a COMBAR report. This value of two miles is within the limits of accuracy of rectification.

The single pressure trace of Fig. 19 is from the only station in the network that showed evidence of significant variation in pressure prior to 1400 CST. The rise in pressure was associated with the only reported shower at that time. The showers within the mass of radar echoes had evidently been located between stations in the U. S. Weather Bureau recording precipitation network since the records of hourly accumulation indicate no precipitation prior to 1400 CST. A composite time study of

the SPS radar---echo photographs shown in a previous report by Whitney and Fritz (1961)---indicated that the line of echoes remained approximately fixed, while individual echoes moved northeastward, a direction approximately parallel to the orientation of the line. A study of the pictures for the period prior to 1500 CST viewed at normal projection speed showed development occurring at the southwest end of the line and a dissipation at the northeast end.

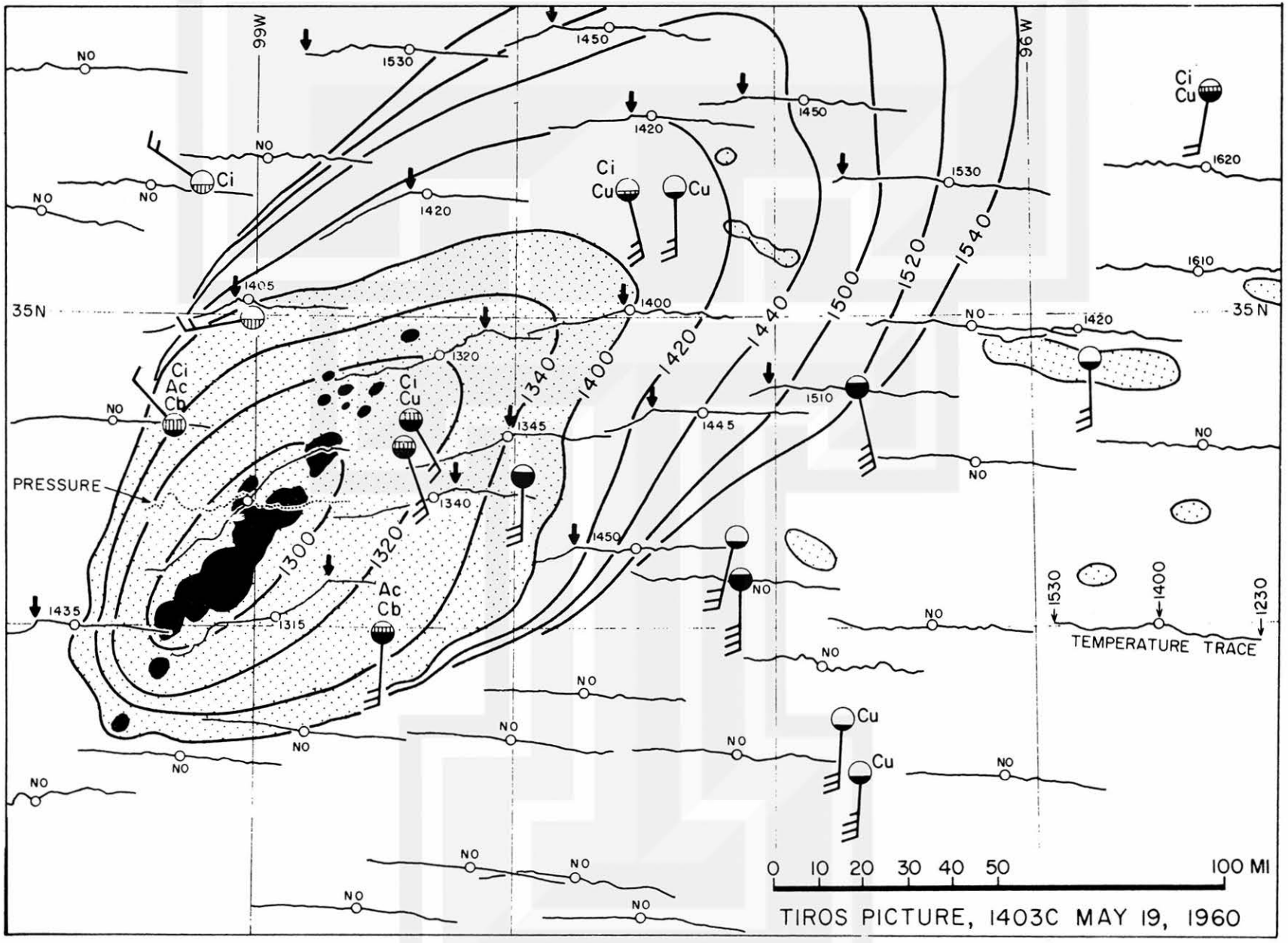

Fig. 19 Isochrones of temperature-drop due to cloud shadow. From Fujita, 1962

VI. DETAILED ANALYSIS OF THE INCIPIENT STAGE

To investigate the possible causes of development during the incipient stage, a detailed surface analysis of all available data was made. To reduce the network temperature and moisture data to a common plane, an analysis was made of the 18-hr mean temperatures and dew points. These were computed from the hourly reports of the regular observing stations. In addition, an analysis was made of the range in temperature and dew point of these stations. The areal means of the 18-hr temperature record and computed dew-point record of the network stations were then fixed by the space distribution of computed means from the regular stations. A check of the distribution of the temperature and dew-point range recorded by network stations indicated only one faulty instrument. That station was not used in the final analysis. The synoptic temperatures and dew points of all the stations were then plotted and analyzed for half-hour intervals from 1300 to 1500 CST.

To extract the maximum amount of information from the radar photographs of the echoes associated with the square-looking cloud pattern, a study was made of the individual characteristics of the line of radar echoes observed by the SPS radar during the period 1305 through 1458 CST. From the study of the PPI photographs taken at two to three minute intervals, areas of corresponding echoes were followed in an attempt to compute their motion and time changes. From the computed motions and changes in areas it was found that the PPI presentation of these echoes as a solid line was the result of the large beam width of the radar, approximately 3.5 degrees, and a high gain setting. On the plot of the movement of these characteristic areas individual echoes were approximated with their angular dimension reduced to fit a beam width of approximately 0.5 degrees. The development and dissipation at the ends of the line of echoes then became evident. Figure 20 is a time plot of the reduced echoes showing the motion and characteristic changes in area at approximate half-hour intervals during the period of detailed study. The points where the horizontal line intersects the vertical lines are the location of the SPS radar in the time scale. The space scale indicates the resulting sizes of the portrayed echo elements. As can be

seen in Fig. 20 the continuity of these reduced echoes could be followed throughout the period of detailed analysis.

Figures 21 and 22 are the composite presentations of the resulting analyses for 1300 and 1400 CST. In Fig. 21 the region between the moisture front and the temperature front is influenced by a high surface temperature and a large gradient in dewpoint temperature. Although the values of temperature are derived from the computed means, the gradients of temperature should be realistic since the means do not effect the gradient. Note that the location of the radar echoes is between adjacent stations in the network (Fig. 19); therefore, the lowered temperature due to the cloud shadow is not evident in the station data at 1300 CST. The moisture front is located west of the largest radar echo and essentially in the region of echo development.

Although there were no detailed upper air measurements, this proximity of convective activity to the moisture front resembles that reported by Fujita (1958). In his study the vertical motion field showed upward motion in the moist region and downward motion in the dry region. In both that study and the dry front case studied by Omoto (1958), the fronts were moving as dry fronts; whereas in this study the moisture front (as indicated by the network data), if moving at all, was moving imperceptibly. These imperceptible motions of the moisture front at the southwest end of the line of echoes could be the triggering mechanism for the development of the echoes. The sparsity of surface wind data in this region for the whole study precluded conclusions regarding the greater surface convergence necessary for the instigation of vertical motion in this region as compared to other regions along the temperature front. However, the composite study of the temperature and moisture fields (shown in the overlays) of 1300 CST indicates that the effects of uneven surface heating (the hot spot in the temperature field), which could instigate vertical motions, and the resulting surface convergence in a small area including the area of high moisture, would be sufficient to initiate the cloud pattern as shown by the rectified TIROS picture for 1400 CST (Fig. 22 - blue overlay).

As can be seen in Fig. 19, the 1300 CST isochrone of temperature drop due to the cloud shadow encompassed only one station in the NSSP network. It was this particular station (L-17 in the NSSP, alpha network) that registered the highest temperature (prior to the shadow effect) of all stations finally effected by the cloud shadow.

Although station spacing is concerned in the following statement, it is interesting that L-17 was the first station in the network to record precipitation, which began at approximately 1300 CST.

When viewed in the composite presentation of Fig. 22, some interesting relations between the temperature and moisture fields and the cloud cover become evident. Although the region of clouds in the northwest corner of the map is near the boundary of the network, the effect of the southward protruding cloud mass in southwestern Kansas on the surface temperature field is a decided cooling. The change in moisture gradient eastward from beneath this cloud mass effectively produces an increase in the relative humidity near the eastern border of the protruding mass. Since the wind speeds in this region, shown by the plotted winds on the base chart, are high relative to the surrounding region, the effect of the partial cooling due to cloud shadow is noted to the south. The temperature decrease due to the shadow effect of the cloud masses east of the square-looking cloud is less explicit than in the case of the previous two cloud masses. This is mainly due to the differences in the degree of opacity indicated by the light stippling which refers to not totally opaque clouds. The clear region between the square-looking cloud mass and the southward protruding cloud mass is believed to have been photographed by the narrow angle camera of TIROS I. These photographs indicated that small cumulus clouds were scattered throughout the relatively moist region north of the temperature front.

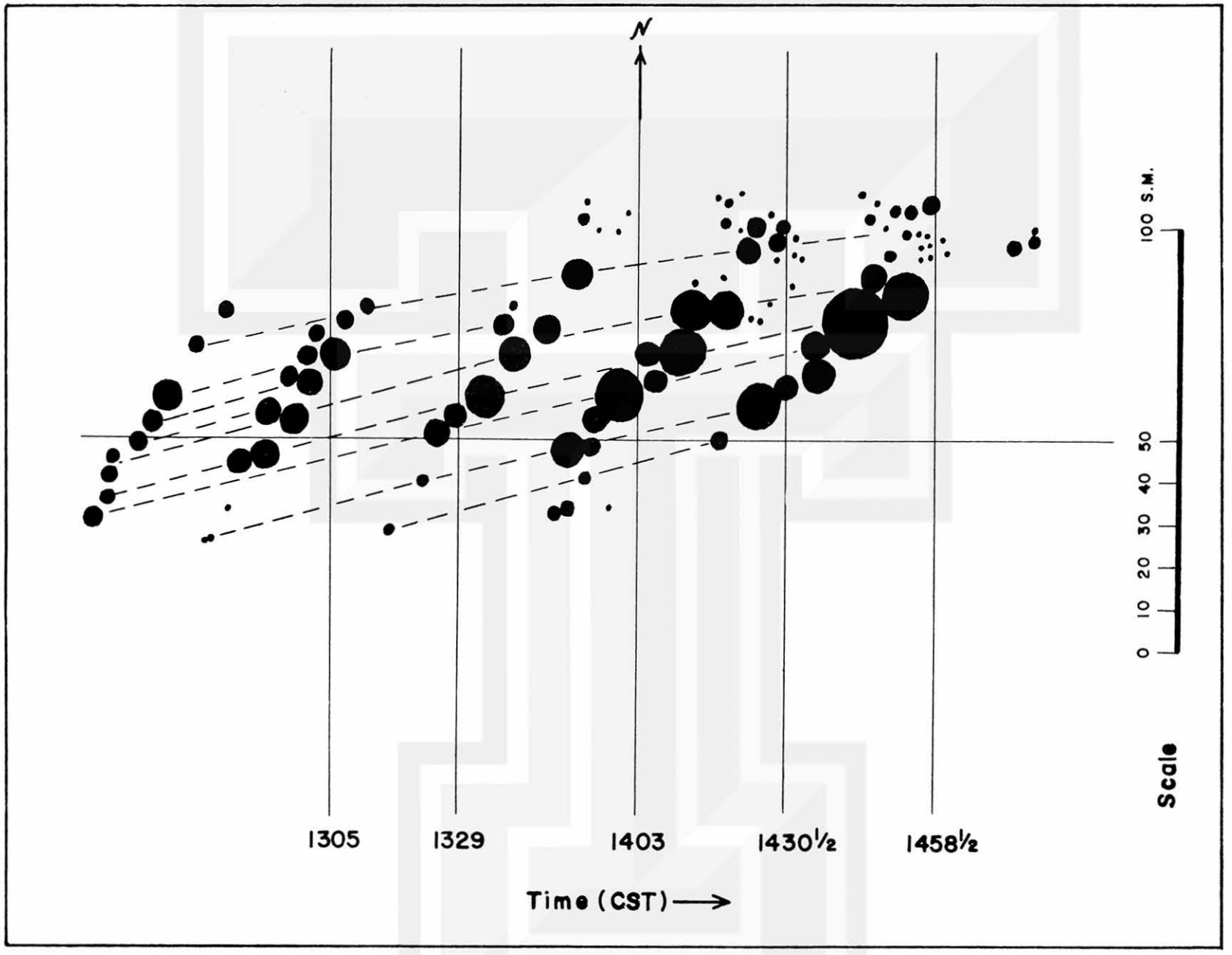

Fig. 20 Composite time plot of the reduced SPS radar echoes. Time increases from left to right. The intersections of the horizontal with the vertical lines denote the positions of SPS relative to the corresponding echoes. The vertical lines point to true North. Space scale is valid synoptically.

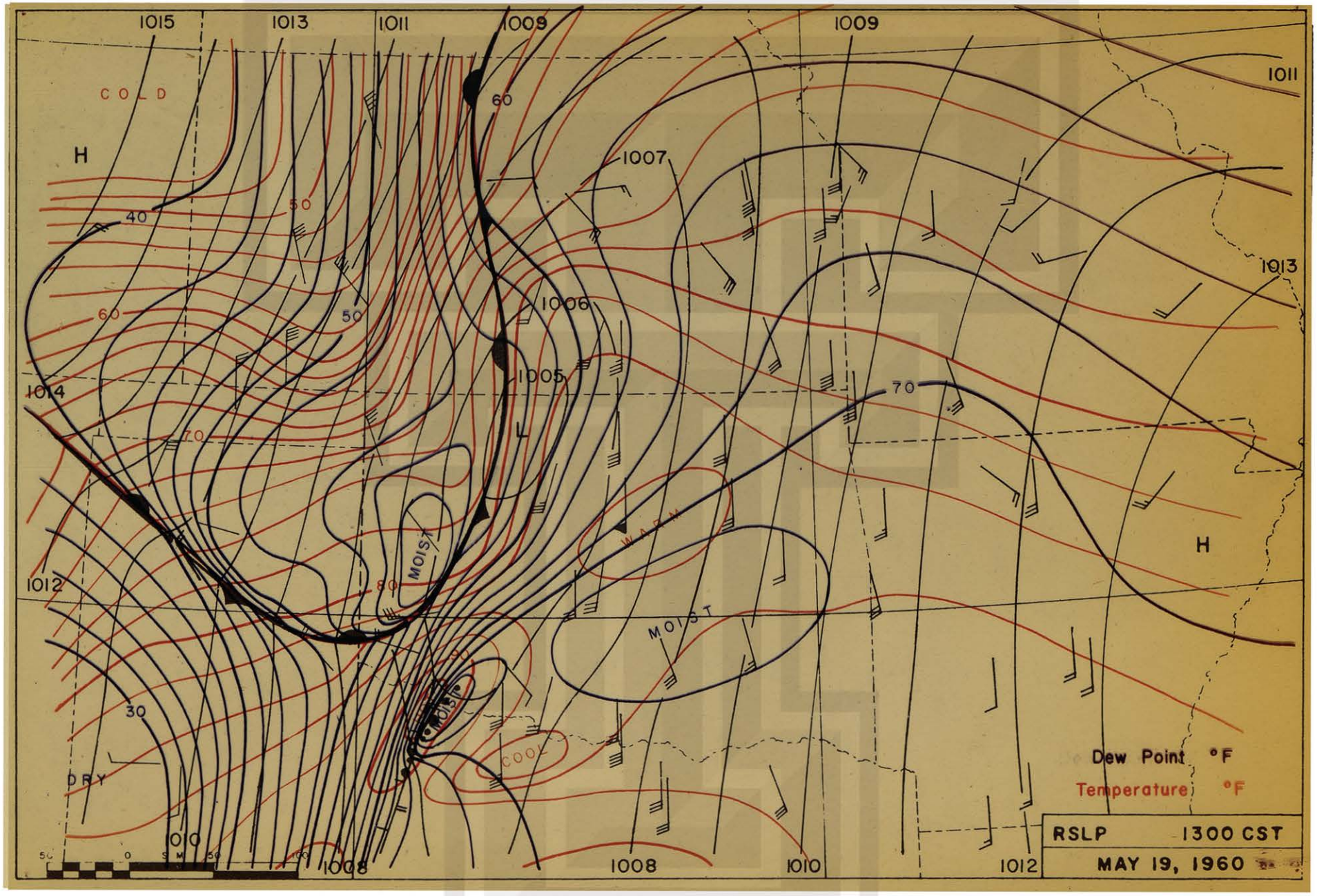

Fig. 21 Composite analyses for 1300 CST. Base chart is reduced sea level pressure, winds, and fronts with reduced SPS radar echoes (1305 CST) indicated by the solid areas. Isotherms (red overlay) are drawn for intervals of 2°F. Isodrosotherms (blue overlay) are drawn for intervals of 2°F.

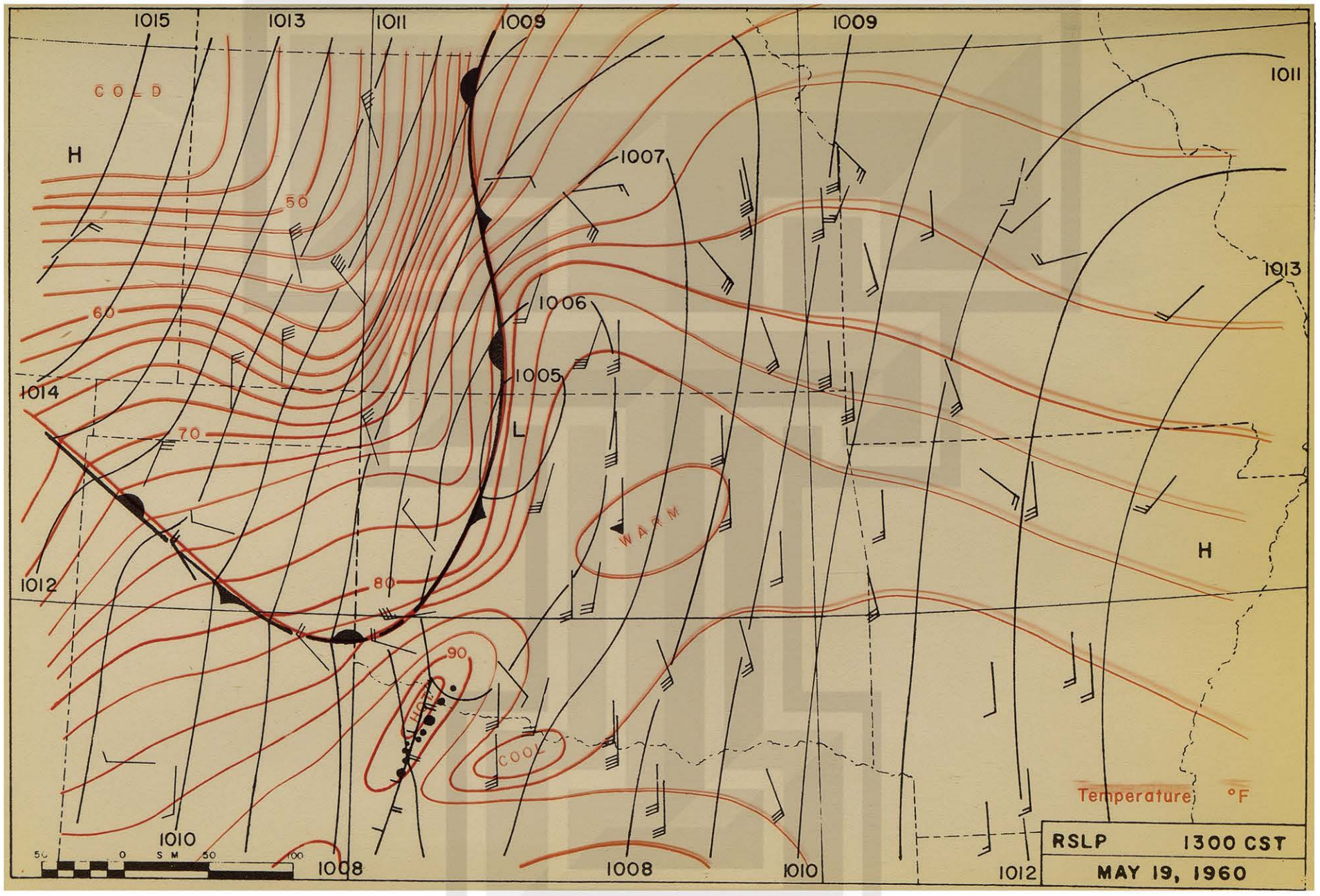

Fig. 21 Composite analyses for 1300 CST. Base chart is reduced sea level pressure, winds, and fronts with reduced SPS radar echoes (1305 CST) indicated by the solid areas. Isotherms (red overlay) are drawn for intervals of 2°F. Isodrosotherms (blue overlay) are drawn for intervals of 2°F.

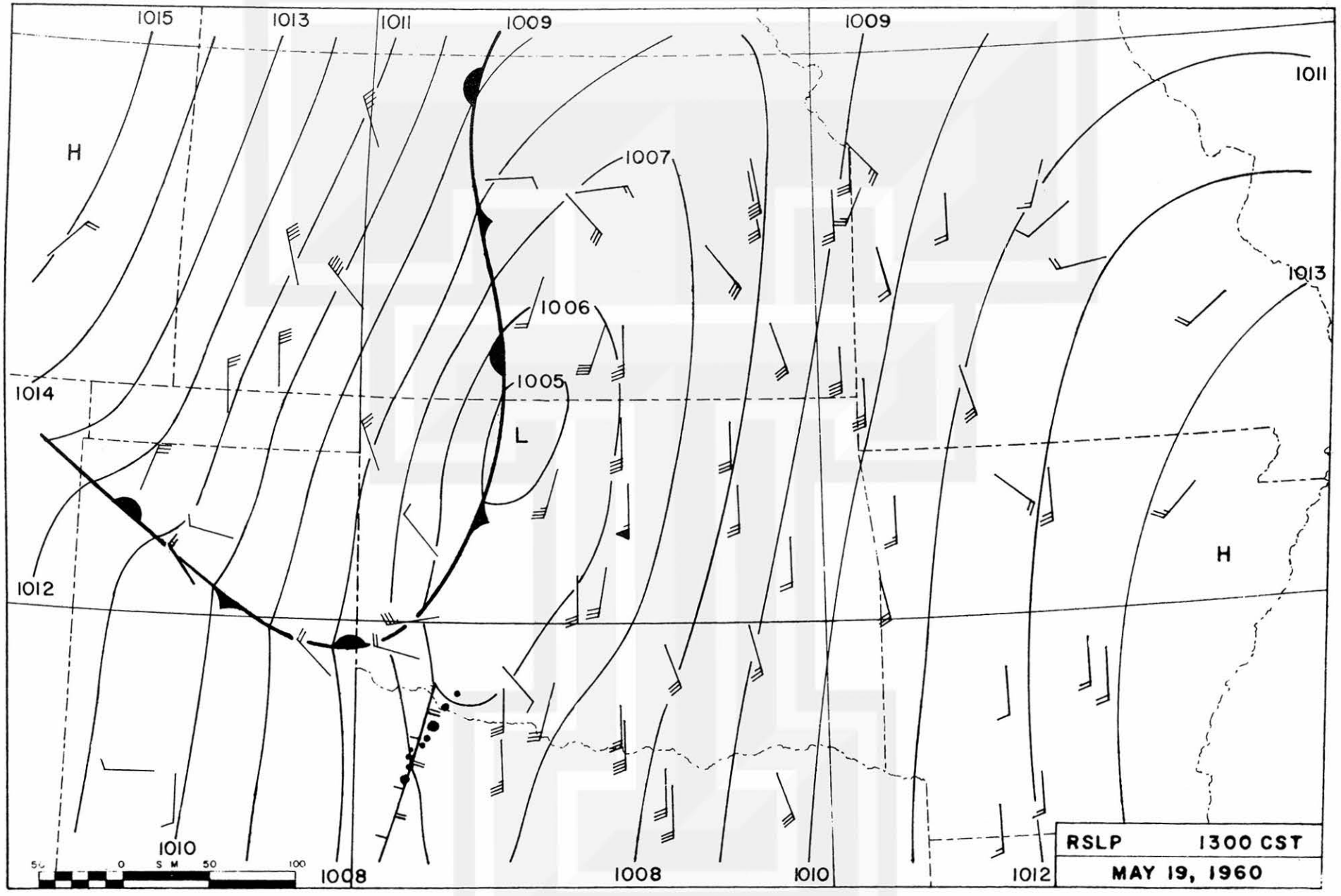

Fig. 21 Composite analyses for 1300 CST. Base chart is reduced sea level pressure, winds, and fronts with reduced SPS radar echoes (1305 CST) indicated by the solid areas. Isotherms (red overlay) are drawn for intervals of 2°F. Isodrosotherms (blue overlay) are drawn for intervals of 2°F.

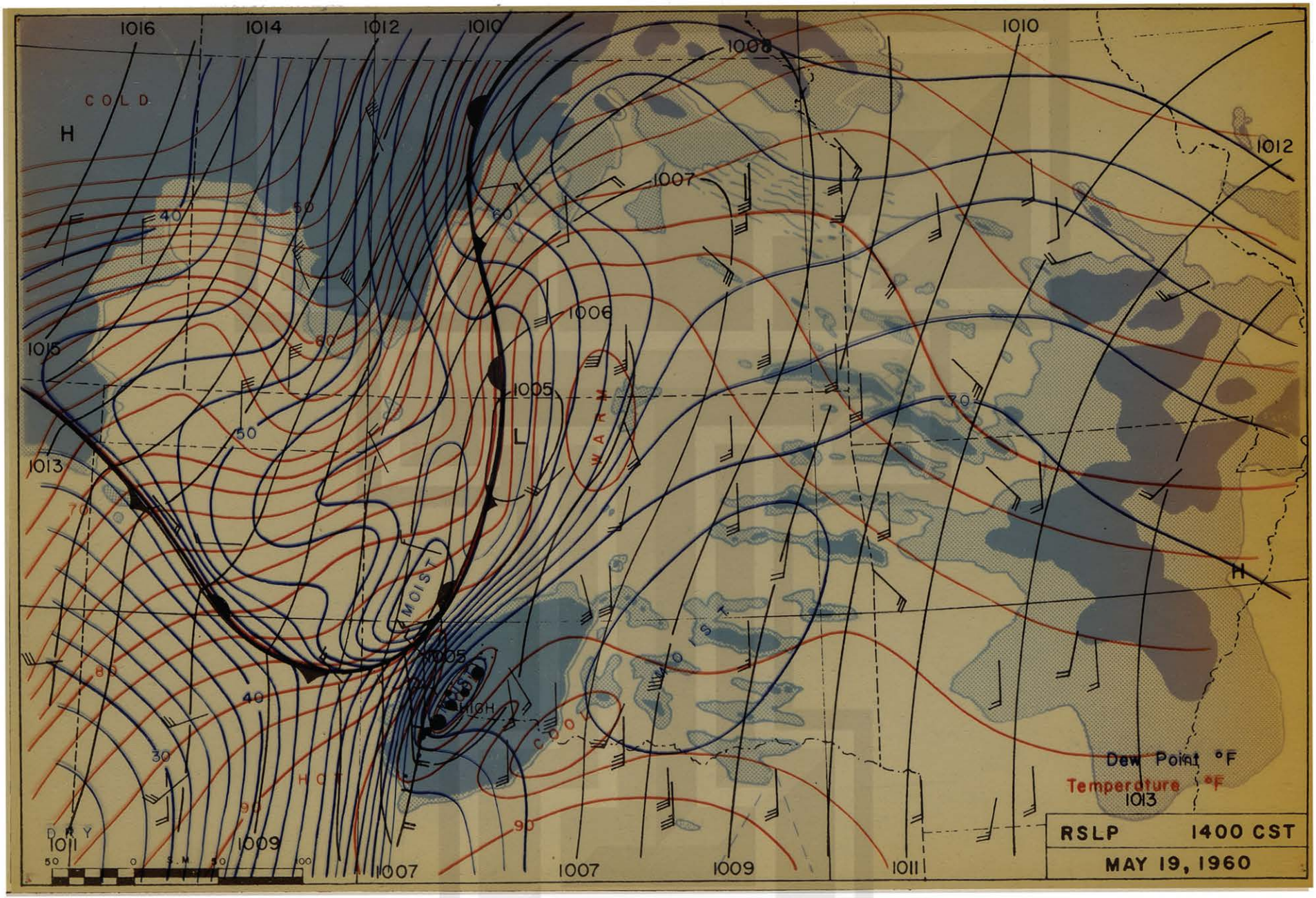

Fig. 22 Composite analyses for 1400 CST. Base chart is reduced sea level pressure, winds, and fronts with reduced SPS radar echoes (1403 CST) indicated by the solid areas. Rectified TIROS photographed cloud masses (light blue overlay) appear as solid areas (opaque clouds) and stippled areas (not totally opaque clouds). Isotherms (red overlay) are drawn for intervals of 2°F. Isodrosotherms (dark blue overlay) are drawn for intervals of 2°F.

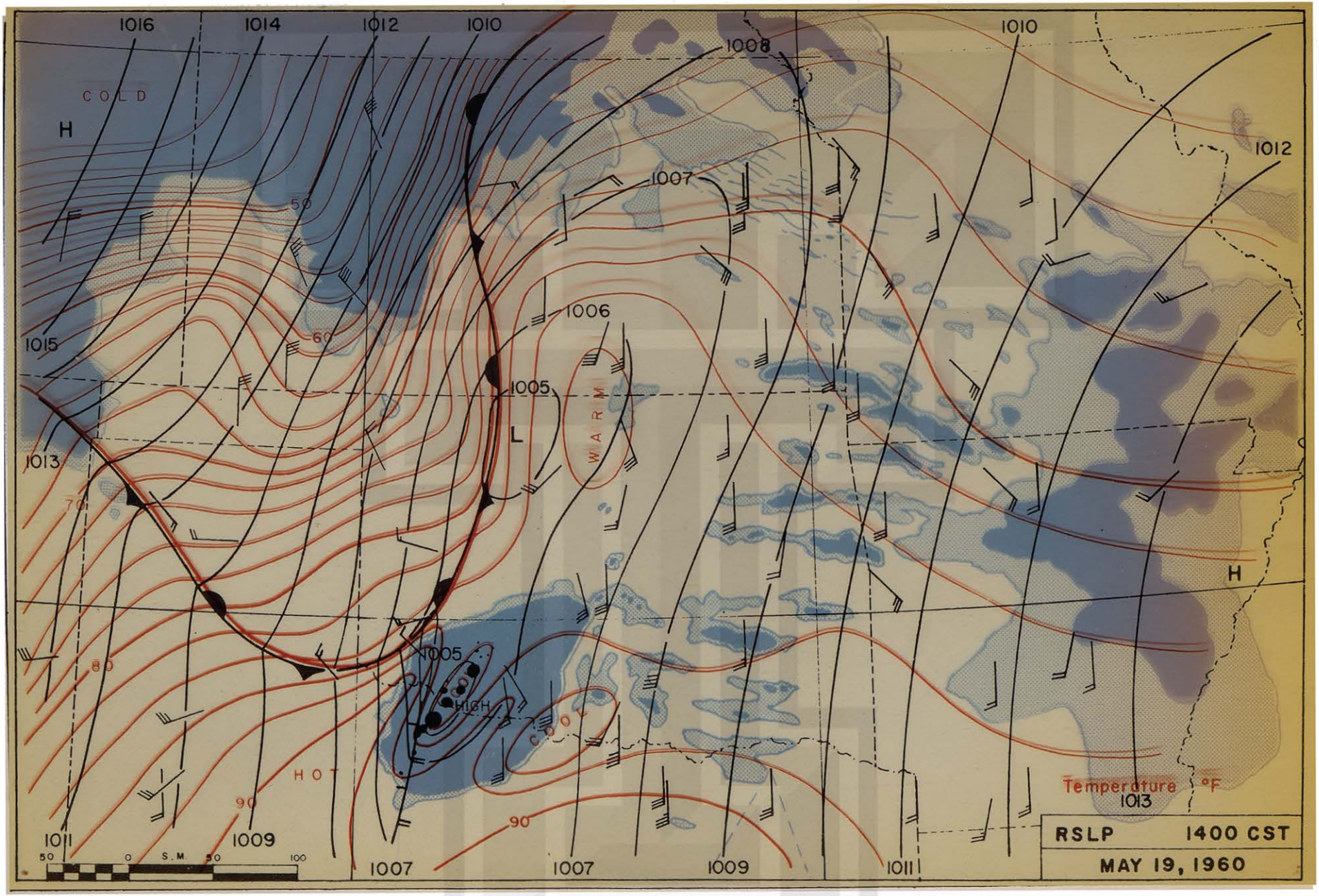

Fig. 22 Composite analyses for 1400 CST. Base chart is reduced sea level pressure, winds, and fronts with reduced SPS radar echoes (1403 CST) indicated by the solid areas. Rectified TIROS photographed cloud masses (light blue overlay) appear as solid areas (opaque clouds) and stippled areas (not totally opaque clouds). Isotherms (red overlay) are drawn for intervals of 2°F. Isodrosotherms (dark blue overlay) are drawn for intervals of 2°F.

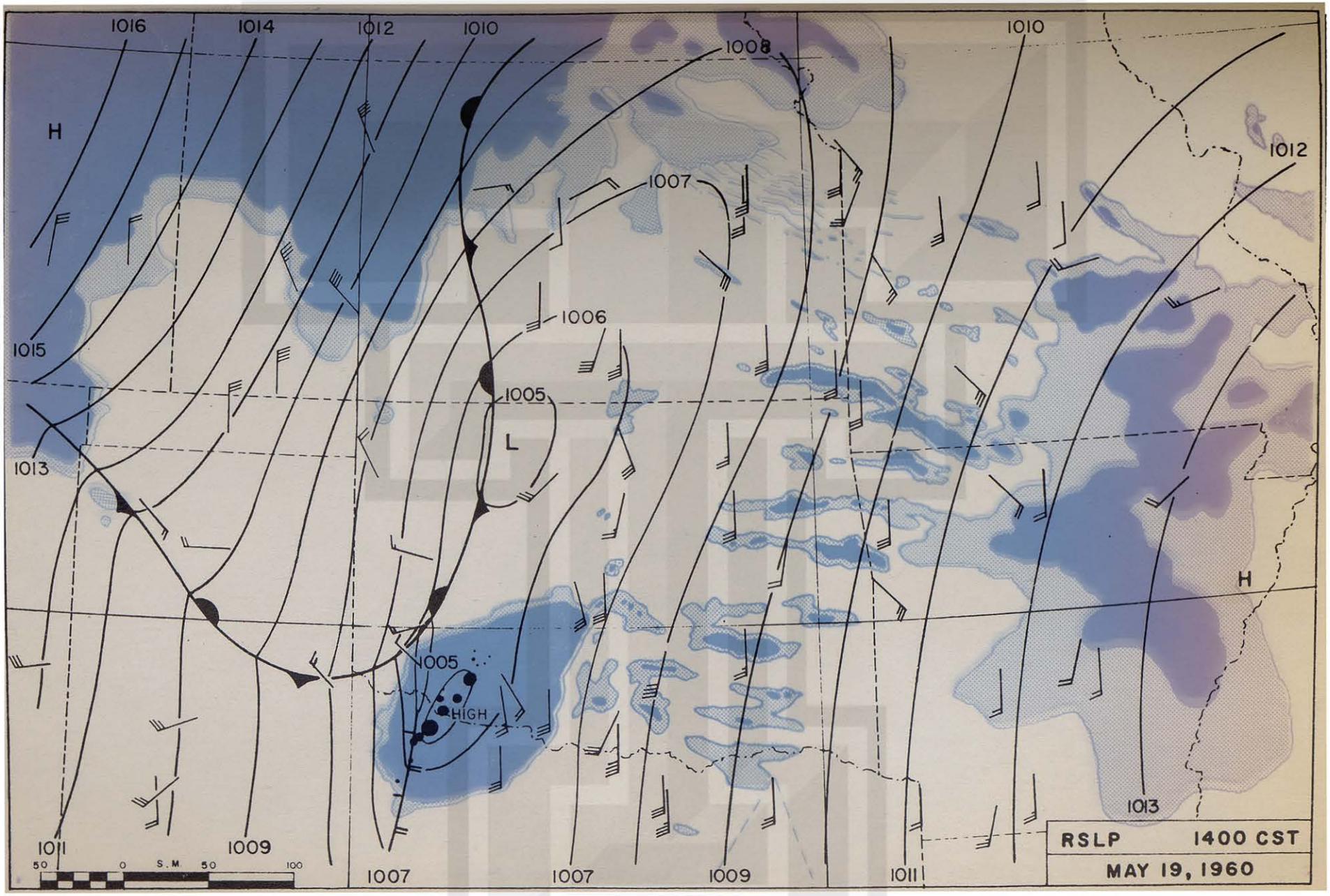

Fig. 22 Composite analyses for 1400 CST. Base chart is reduced sea level pressure, winds, and fronts with reduced SPS radar echoes (1403 CST) indicated by the solid areas. Rectified TIROS photographed cloud masses (light blue overlay) appear as solid areas (opaque clouds) and stippled areas (not totally opaque clouds). Isotherms (red overlay) are drawn for intervals of 2°F. Isodrosotherms (dark blue overlay) are drawn for intervals of 2°F.

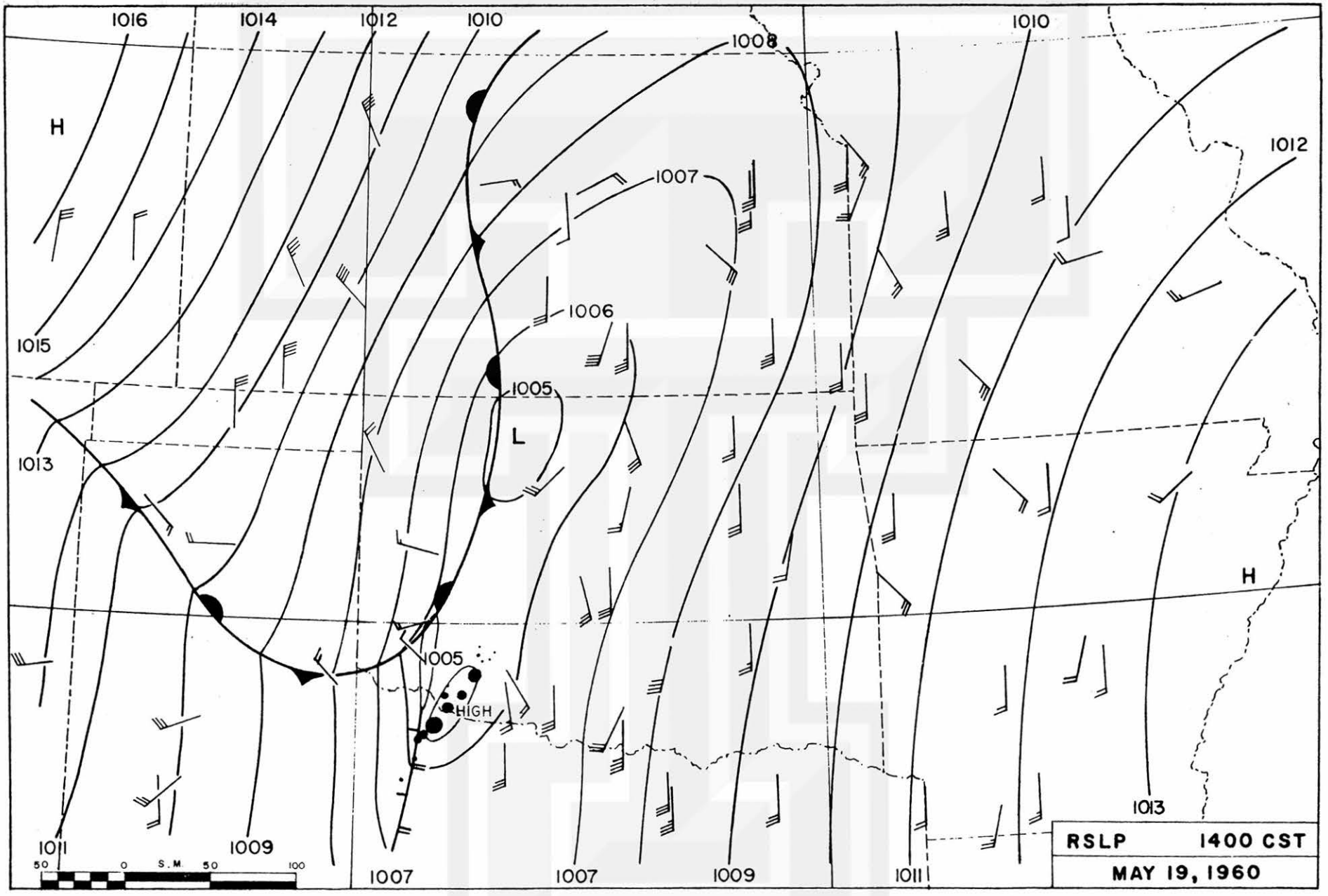

Fig. 22 Composite analyses for 1400 CST. Base chart is reduced sea level pressure, winds, and fronts with reduced SPS radar echoes (1403 CST) indicated by the solid areas. Rectified TIROS photographed cloud masses (light blue overlay) appear as solid areas (opaque clouds) and stippled areas (not totally opaque clouds). Isotherms (red overlay) are drawn for intervals of 2°F. Isodrosotherms (dark blue overlay) are drawn for intervals of 2°F.

VII. APPROXIMATION TO THE DIVERGENCE AT 1400 CST

On the plot of smooth curves representing the local wind changes of Fig. 6, hourly positions of the wind vector were approximated (see Fig. 6 B). These positions were interpolated using a number of qualitative factors. The hourly values of wind at each grid point were approximated using a spacing consistent with a continuous acceleration at data times. In cases where an increase or decrease of the maxima or minima in the isotach pattern was implied between data times, these increases and decreases were made in a manner consistent with time and space continuity. Figure 23 is the approximated pattern of streamline and isotachs for the 200-mb surface at 1400 CST. As a means of checking the order of magnitude of the divergence computed from the approximated wind field of 1400 CST near the area of the square-looking cloud, the percent rate of change of area of the cloud mass was computed from the isochrones of Fig. 19.

With regard to the kinematics in the expansion of the cloud mass, the wind field in the region of the cloud mass during the period of the temperature drop is considered to be similar to the resultant field of a group of moving point sources and pure translation. From the detailed study of the radar echoes, it was noted that the direction of motion of the discernible individual echoes was approximately the same throughout the period 1300-1500 CST. It was also noted that development was occurring at the southwest end of the line of echoes and dissipation at the northeast end. Therefore, the upwind growth of the anvil tops implied by the southwestward extension of the isochrones at the southwest end of the square-looking cloud mass could be largely the result of new development in this region. Although the strengths of individual sources in the field were most likely varying (i. e., in the scale normally the concern of cloud physicists), it is assumed that the total effect of these changing source strengths is a line source increasing in strength and increasing its length southwestward from 1300 to 1400 CST and then remaining a constant line source of fixed length through 1500 CST. The spreading of the cloud mass toward the southeast and northwest is probably due to the increasing source strength.

A perusal of the temperature changes related to the cloud shadow will show that there was generally a more abrupt change in temperature and a larger temperature drop associated with the isochrones near 1300 CST than with the isochrones of later times. This could be explained by the degree of opacity of the cloud mass as determined by mixing. It is likely that the combined effects of areal expansion of the cloud mass with increased distance from the source were to increase with time the amount of mixing at the edge of the cloud mass. This increased mixing effect would then contribute to an underestimate of the expansions at later times. It was assumed that the underestimation of the velocity divergence due to mixing and the overestimation due to the seemingly large upwind growth of the anvil tops would cancel one another.

In addition to checking the previous conjectures regarding the kinematics, the divergence was computed for differing time intervals to note any effect of the finite difference approximation to the mathematical infinitesimal time dt in the relation

$$\frac{1}{A} \cdot \frac{dA}{dt} = \text{div } \mathbf{V}$$

where A is the area undergoing change during the time, dt, and $\mathbf{V}$ is the wind velocity measured at the constant pressure surface. In Table I are the changes in area over differing time intervals measured by planimetry and the resulting values of divergence.

Time	δA (20 min.)	div. 10^{-4} sec^{-1}	δA (40 min.)	div. 10^{-4} sec^{-1}	δA (80 min.)	div. 10^{-4} sec^{-1}	δA (120 min.)	div. 10^{-4} sec^{-1}
1300								
	2.27	10.3						
1320			4.89	6.1				
	2.62	4.7						
1340			5.65	4.0	11.16	3.9		
	3.03	3.4						
1400			6.27	2.9	12.13	2.8	17.75	2.8
	3.24	2.6						
1420			6.48	2.2	12.86	2.2		
	3.24	2.0						
1440			6.59	1.8				
	3.35	1.6						
1500								

Table I. Divergence computed from the area integration of the temperature-drop isochrones.

As can be seen in Table I, the greater increases in $\bar{\delta}A$ (per 20 minutes) with time prior to 1400 CST seems to bear out the assumption of an increasing source strength during the period 1300-1400 CST. The divergence is decreasing rapidly due to the area factor. Concerning the finite difference approximation to the mathematically infinitesimal time increment, the value $2.9 \times 10^{-4} sec^{-1}$ seems to be appropriate for the instantaneous divergence at 1400 CST regardless of the time increments used. When this value is compared to that computed from the approximated wind field, it is seen that the approximated divergence is less by greater than one order of magnitude. If a comparison were made between the 1800 CST divergence at 200 mb in the region of the mesosystem, and the value computed from the isochrones for 1400 CST, the difference would again be one order of magnitude. In fact the only data time, for which divergence at 200 mb was computed, that was comparable (within one order of magnitude) was 2400 CST (Fig. 24). The streamlines, isotachs, and isopleths of divergence in this figure are represented as in Fig. 23, and the surface boundaries of the two systems are indicated by heavy dashed lines. The distribution of upper air stations reporting at 2400 CST can be seen in the report by Goldman and Fujita (1961). The relatively smooth decrease of divergence eastward is due to approximations made in the absence of adequate data in the region east of the second mesosystem. However, the large values of divergence relating to the second mesosystem are believed to be adequately determined from the data.

Considering the many assumptions made concerning the kinematics relating to the cloud mass growth and the assumptions involved in the approximation of hourly wind variability, an evaluation of the method of approximation based on the values derived from the cloud mass growth would be impossible. Supplementing reported data with the use of established models of the wind field was contemplated; however, most of the models that were related to large scale surface patterns would not be applicable to the large scale surface pattern of May 19, 1960. Of the few that could be applied, none were in any fashion related to severe storms or other mesoscale disturbances. It seems, therefore, that the evaluation of both the approximation technique and the applicability of data derived from the cloud mass growth to kinematics in the mesoscale must await more detailed measurements.

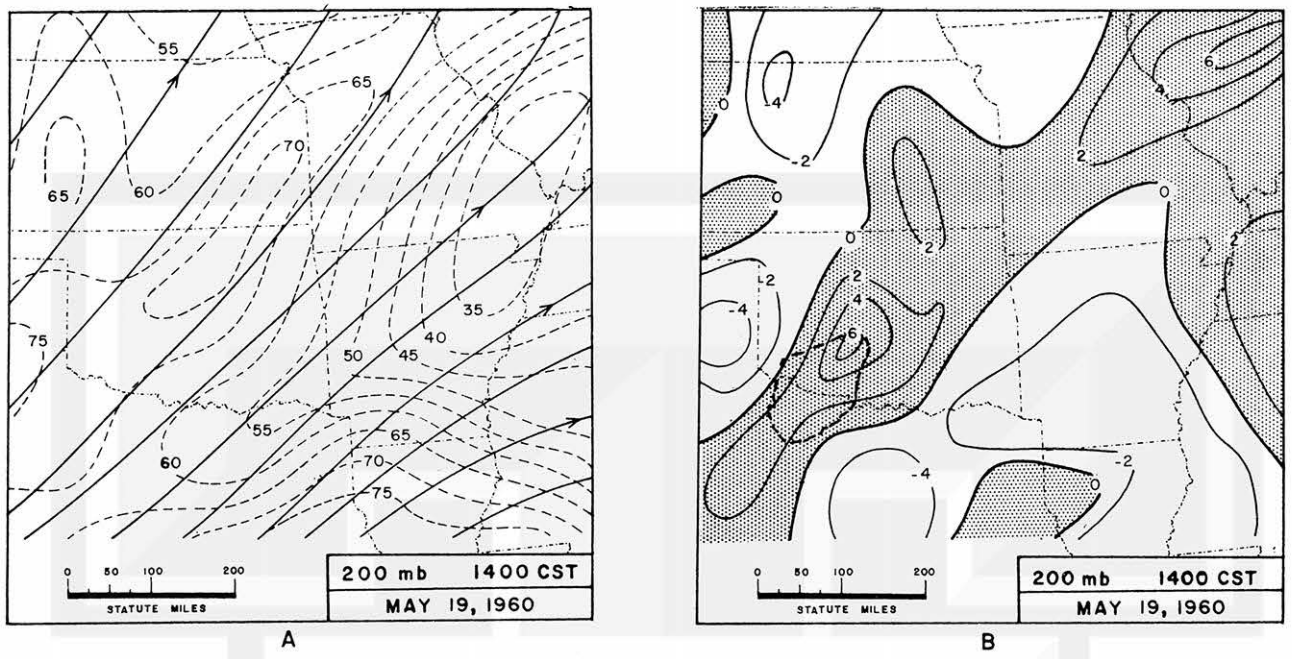

Fig. 23 Approximation to the upper air kinematics at 1400 CST. A - Approximated streamlines (solid) and isotachs (dashed lines) at 5-kt intervals. B - Isolines of divergence ($x10^{-5}$ sec^{-1}). Region of positive divergence is stippled and outline of rectified cloud mass is dashed.

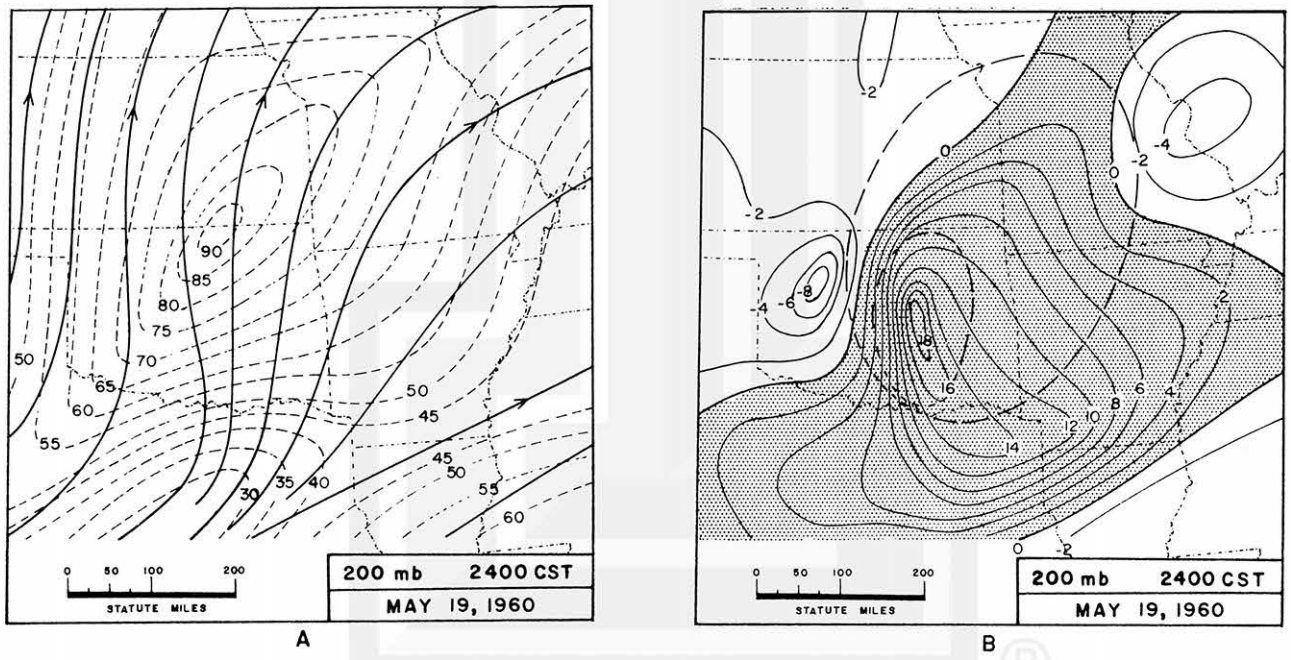

Fig. 24 Upper air kinematics. A - Streamlines (solid) and isotachs (dashed lines) at 5-kt intervals. B - Isolines of divergence ($x10^{-5}$ sec^{-1}) with surface boundary of mesosystems (dashed lines), stippled area is region of divergence.

VIII. CONCLUSIONS AND SUGGESTIONS FOR FUTURE RESEARCH

With the use of all the meteorological data for May 19, 1960, a definitive model of the four dimensional processes involved in mesoscale circulation can only be represented qualitatively. Knowledge of the hourly variation of upper winds is a necessity, if quantitative changes in the dynamics of systems are to be studied. The study of the incipient stage of the mesosystem was greatly enhanced by the TIROS photographs; however, until details are known regarding the kinematics and physical processes of the clouds appearing in satellite photographs, any detailed information derived from TIROS photographs will be limited to the results presented in this study.

The sferics data studied for this case showed evidence of electrical activity in the general region of the mesosystems examined. From the results presented by Samson and Linfield (1962) for a single station, sferics data could aid in the location of regions of maximum activity within a mesosystem if the resolution is greater than the indicated six degrees azimuth. From the plots of triangulated regions of sferics activity, no additional information regarding the physical characteristics of the mesosystems could be obtained. However, this is not meant to imply that sferics data is not useful. The capability of sferics to detect severe storms at long range is obviously useful in regions lacking other data.

It is concluded from the computation of the profiles of vertical motion that details of the mesosystem itself could not be determined from the upper air data available in 1960. Although some effects of a circulation which is smaller than cyclone scale were shown in the profiles, these effects are believed to be due to the adjustment of the atmosphere to the existence of a mesoscale perturbation imbedded in it. This adjustment is shown locally by the slight decrease in pressure preceeding the surge line, or as the remaining surface pressure pattern when excess pressure is subtracted from the pattern (Goldman, 1961). Quantitative descriptions of both the adjustment of the atmosphere to the perturbation and the perturbation itself must await more detailed measurements.

During the two year interim from May, 1960, to the present, there has been a concerted effort by the NSSP to obtain more detailed surface and upper air data. With the use of more than one aircraft, upper air measurements in and near regions of convective activity have been made. As an additional aid to the study of mesoscale changes in the structure of convective systems, cloud photographs which can be rectified precisely are being taken from these aircraft with the cooperation of the Mesometeorology Project, U. of Chicago. With the use of photogrammetric techniques, the short term variations of mesoscale circulation, as represented by the three dimensional changes in cloud systems, should prove a useful tool in the study of this circulation. To aid in the study of the incipient stage of mesosystems as well as the detailed structure of well defined systems, the NSSP instrumented a dense surface network (Fujita, 1961) located within the existent alpha network, and increased the number of times individual radiosonde stations within and in the proximity of the alpha network make soundings. In addition, dropsondes should help to implement the density of upper air stations.

With the use of aerial photogrammetric techniques that allow a precise study of cloud to shadow relationships, and a network with station density of the NSSP beta network, it is believed that the influence of surface heating on the incipient stage of severe storms could be studied quantitatively. In addition, such a study may aid in the interpretation of satellite radiation measurements, which recently have been shown to be significant in the mesoscale (Fujita, et al., 1962).

In the past and in this study, efforts have been made to devise techniques by which mesoscale analyses describing physical processes could be made from data too widely spaced in both time and space to be handled by conventional synoptic meteorological techniques. It is hoped that in the future data measured with the intent of the description of mesoscale phenomena will continually be made available for detailed study of the physical processes in severe storms.

ACKNOWLEDGEMENTS

In addition to those individuals who contributed their efforts to the presentation of the preliminary report, the author gratefully acknowledges the many discussions on techniques and theory with Dr. Tetsuya Fujita. Without the analysis and rectification techniques that he had developed, a significant portion of this study could not have been made.

REFERENCES

Fujita, T., 1955: Results of detailed synoptic studies of squall lines. Tellus 7, 4, 405-436.

----------, 1958: Structure and movement of a dry front. Bull. Amer. Meteor. Soc. 42, 574-582.

----------, 1961a: Index to the NSSP surface network. Res. Paper 2, Mesomet. Proj., U. of Chicago.

----------, 1961b: Outline of a technique for precise rectification of satellite cloud photographs. Res. Paper 3, Mesomet. Proj., U. of Chicago.

----------, 1962: A review of researches on analytical mesometeorology. Res. Paper 8, Mesomet. Proj., U. of Chicago.

----------, T. Ushijima, W. A. Hass, and G. T. Dellert, Jr., 1962: Meteorological interpretation of convective nephsystems appearing in TIROS cloud photographs. Res. Paper 9, Mesomet. Proj., U. of Chicago.

Goldman, J. L., 1961: An investigation of development processes of the wake depression through excess pressure analysis of nocturnal showers. Res. Paper 5, Mesomet. Proj., U. of Chicago.

----------, and T. Fujita, 1961: Study of developmental processes of severe storms using satellite and terrestrial based observations. Preliminary Report: Reduced data for the square cloud case, May 19, 1960. Rep. to USWB under Contract Cwb 9931.

Omoto, Y., 1958: Study of outbreaks of severe local storms near dry fronts. Tech. Rep. 4, USWB, Contract Cwb 9321, Aug., 1958.

Panofsky, H. A., Albert Miller, Robert Curtis, Raymond Deland, and David L. Jones: Properties of vertical motion. Sci. Rep. No. 1, Contract No. AF 19(604)-1025. The Pennsylvania State University.

Petterssen, S., 1956: Weather Analysis and Forecasting, McGraw-Hill Book Co. Inc., New York, p. 133.

Samson, C. A., and R. F. Linfield, 1962: Sferic observations of severe weather on May 19, 1960. Jour. Geophy. Res. 67, 627-635.

Whitney, L. F., Jr., and S. Fritz, 1961: A tornado-producing cloud pattern seen from TIROS I. Bull. Amer. Meteor. Soc. 42, 603-614.

MESOMETEOROLOGY PROJECT ---- RESEARCH PAPERS

1. Report on the Chicago Tornado of March 4, 1961 - Rodger A. Brown and Tetsuya Fujita

2. Index to the NSSP Surface Network - Tetsuya Fujita

3. Outline of a Technique for Precise Rectification of Satellite Cloud Photographs - Tetsuya Fujita

4. Horizontal Structure of Mountain Winds - Henry A. Brown

5. An Investigation of Developmental Processes of the Wake Depression Through Excess Pressure Analysis of Nocturnal Showers - Joseph L. Goldman

6. Precipitation in the 1960 Flagstaff Mesometeorological Network - Kenneth A. Styber

7. On a Method of Single- and Dual-Image Photogrammetry of Panoramic Aerial Photographs - Tetsuya Fujita

8. A Review of Researches on Analytical Mesometeorology - Tetsuya Fujita

9. Meteorological Interpretation of Convective Nephsystems Appearing in TIROS Cloud Photographs - Tetsuya Fujita, Toshimitsu Ushijima, William A. Hass, George T. Dellert, Jr.